Geoscientific
Model Development
Discussions

The Brazilian Earth System Model version 2.5: Evaluation of

its CMIP5 historical simulation

Sandro F. Veiga[1], Paulo Nobre[2], Emanuel Giarolla[3], Vinicius Capistrano[4], Manoel Baptista Jr.[2], André L. Marquez[2], Silvio Nilo Figueroa[2], José Paulo Bonatti[2], Paulo Kubota[2], Carlos A. Nobre[5]

[1]Earth System Science Center-CCST, National Institute for Space Research (INPE), São José dos Campos 12227-010, São Paulo, Brazil

[2]Center for Weather Forecasting and Climate Studies-CPTEC, National Institute for Space Research (INPE), Cachoeira Paulista 12630-000, São Paulo, Brazil

[3]Center for Weather Forecasting and Climate Studies-CPTEC, National Institute for Space Research (INPE), São José dos Campos 12227-010, São Paulo, Brazil

[4]Amazonas State University (UEA), Manaus 69005-010, Amazonas, Brazil

[5]CN Research, São José dos Campos 12544-590, São Paulo, Brazil

Correspondence to: Sandro F. Veiga (sandro.veiga@inpe.br)

1   **Abstract**

2

3   The performance of the coupled ocean-atmosphere component of the Brazilian Earth

4   System Model version 2.5 (BESM-OA2.5) simulating the historical period 1850-2005 is

5   evaluated. Following climate model validation procedure, in which the atmospheric and

6   oceanic main variabilities are validated against observation and Reanalysis datasets, the

7   evaluation particularly focuses the mean climate state and the most important large-

8   scale climate variability patterns simulated in the historical run, which is forced by

9   observed greenhouse gas concentration. The most significant upgrades in the model's

10   components are also presented briefly. BESM-OA2.5 is able to reproduce the most

11   important large-scale variabilities, particularly over the Atlantic (e.g. the North Atlantic

12   Oscillation, the Atlantic Meridional Mode and the Atlantic Meridional Overturning

13   Circulation) and the extratropical modes that occur in both hemispheres. The model's

14   ability in simulating large-scale variabilities indicates its usefulness for seasonal climate

15   prediction and climate change studies.

16

1. Introduction

Climate Models and their recent extension to become Earth System Models, by the inclusion of biogeochemical cycles, are key tools to investigate climate phenomena which greatly influence human societies (e.g. von Storch, 2010; Flato, 2011). Since 2008 the Brazilian climate community has been engaged in setting up the Brazilian Earth System Model (BESM; Nobre et al., 2013; Giarolla et al., 2015); a major scientific task which has been carried out by Brazilian scientific institutions invoking the critical need to address reliable future climate projections and their potential impacts, particularly over South America. The primary objective encompassed in this effort is to build up the scientific expertise capable to develop and maintain a state-of-the-art Earth System Model. Such an achievement would represent a significant step forward in establishing a scientific tool which can be used in different arrays of research activities. The importance of such undertaking lies in the understanding of the physics of the Earth system to produce and confer credibility to studies of impacts of climate change in different areas of great importance; such as food and water security, tropical ecosystems, natural disasters, and so on. One of the primordial aims of the BESM project is to participate in the Coupled Model Intercomparison Project's sixth phase (CMIP6; Meehl et al., 2014).

The Brazilian Earth System Model (BESM) has been set up at the Brazilian National Institute for Space Research (INPE). At present, it consists of a land-ocean-atmosphere coupled model, in which the coupling is done through the Flexible Modeling System (FMS) coupler, developed at the Geophysical Fluid Dynamics Laboratory (GFDL) of the National Oceanic and Atmospheric Administration (NOAA).

1 The inclusion of aerosols and atmospheric chemistry components are in the phase of

2 implementation and tests. BESM was firstly evaluated in Nobre et al. (2013). This

3 version showed a significant bias on precipitation in the tropical region, with a deficient

4 representation of precipitation in the Amazon region. In order to improve these aspects,

5 studies were conducted to ameliorate cloud parameterizations over the tropics, which

6 improved the precipitation over the same region and the representation of Convergence

7 Zones over both the Atlantic and Pacific Ocean basins (Bottino and Nobre, 2018). Main

8 changes of the current version relate to BESM's atmospheric model, with modifications

9 in the surface wind field and its parameterizations, described in Capistrano et al. (2018).

10 The updated version presented in this manuscript is BESM-OA2.5.

11 One of primary conceptual aim in developing and improving BESM's

12 parameterizations is to serve as a model to be used from numerical weather prediction to

13 seasonal forecast up to the projection of climate change scenarios in a seamless

14 framework as proposed by Palmer et al. (2008). From the operational point of view,

15 BESM is already being used for extended weather forecast to seasonal climate

16 prediction, as well as for producing global climate change scenarios (Nobre et al., 2013)

17 and to provide atmospheric and oceanic boundary conditions to regional climate models

18 for dynamical downscaling of climate change scenarios (Chou et al., 2014).

19 This overview paper describes the most important developments and

20 improvements in the model components, presenting the simulation of recent past mean

21 climate conditions and major large-scale climate phenomena. In section 2 the BESM-

22 OA2.5 components and experimental design are briefly described; section 3 presents the

23 methodology and the observed data used to evaluate the model; section 4 presents the

1   evaluation of the historical simulation, in which are evaluated the most important

2   atmospheric and oceanic variables regarding to their climatological fields and the

3   prominent large-scale phenomena of the climate system; finally, section 5 presents the

4   summary.

5

6   **2 Model Description and Simulation Experiment Design**

7   **2.1 BESM-OA2.5**

8   The atmospheric component of BESM-OA2.5 is the Brazilian Global

9   Atmospheric Model (BAM; Figueroa et al., 2016) developed at Center for Weather

10   Forecasting and Climate Studies (CPTEC/INPE). It is a primitive equation model with

11   spectral representation with triangular truncation at the wave number 62, corresponding

12   to a grid resolution of approximately $1.875° \times 1.875°$, and 28 sigma levels in the

13   vertical, with uneven increment between the levels, i.e. T62L28 resolution. As

14   mentioned before, it is in the atmospheric component which resides the main

15   differences between BESM-OA2.5 and BESM-OA2.3 (Nobre et al., 2013). The new

16   version shows a key improvement in the energy balance at the top of the atmosphere, by

17   reducing the mean global bias from -20 Wm^{-2} in version BESM-OA2.3 to 2 Wm^{-2} in the

18   current version (Capistrano et al. 2018). Version 2.5 of BESM incorporates the

19   formulation presented in Jiménez et al. (2012) for the representation of the wind,

20   humidity and temperature in the surface layer. The model runs without flux correction

21   or adjustment. The physics parameterizations for the continental processes are based on

22   the Simplified Simple Biosphere Model (SSiB) land surface model (Xue et al., 1991), in

1   shortwave radiation Clirad scheme (Tarasova et al. 2007; Chou and Suarez 1999), in

2   longwave radiation Harshvardhan scheme (Harshvardhan et al., 1987), in Cloud

3   microphysics Ferrier scheme (Ferrier et al. 2002), in the turbulence level 2 module

4   (Mellor and Yamada, 1982), in the gravity wave module (Anthes, 1977), in the deep

5   convection module (Arakawa and Schubert, 1974; Grell and Dévényi, 2002), and in the

6   shallow convection module (Tiedtke, 1983). More details can be found in Figueroa et

7   al. (2016) and in Capistrano et al. (2018).

8   The oceanic component of BESM-OA2.5 is the Modular Ocean Model version

9   4p1 (MOM4p1; Griffies, 2009) developed at GFDL, which includes the Sea Ice

10   Simulator (SIS) built-in ice model (Winton, 2000). There are no changes in the physics

11   parameterizations from those used in BESM-OA2.3. The horizontal grid resolution in

12   the zonal direction is $1°$ and in the meridional direction it varies uniformly from $1/4°$

13   between $10°S$ and $10°N$ to $1°$ of resolution at $45°$ and to $2°$ of resolution at $90°$, in both

14   hemispheres. The vertical resolution has 50 levels with approximately 10 m resolution

15   in the upper 220 m, increasing gradually to about 370 m resolution at deeper levels. The

16   oceanic model spin-up was done in a manner similar to that of Nobre et al. (2013) and

17   Giarolla et al. (2015), in which is begin the spinup run from rest, and the T-S structure

18   of the oceans of Levitus (1982). The initial stage of the ocean model spinup was done

19   over a 13 years period, forced by climatological atmospheric fields (winds, solar

20   radiation, air temperature and humidity, and precipitation). It was then integrated by an

21   additional 58 years period, forced by interannually varying atmospheric fields from

22   Large and Yeager (2009), while the river discharges and the sea ice variables were kept

23   at their respective monthly mean climatological values. The forced ocean model run

1   was used to save the oceanic dynamical and thermodynamical structures in order to be

2   used in the initialization of future coupled model experiments.

3   The atmospheric and oceanic models are coupled via the Flexible Modeling

4   System (FMS) coupler, which was also developed at GFDL and incorporated in

5   MOM4p1. The atmospheric model receives SST and ocean albedo from the ocean and

6   sea ice models at hourly time steps. On the other hand, the oceanic model receives

7   information about freshwater (liquid and solid precipitation), momentum fluxes (winds

8   at 10 m), specific humidity, heat, vertical diffusion of velocity components and surface

9   pressure, all also at hourly time steps. Wind stress fields are computed within MOM4p1

10   using Monin-Obukhov scheme (Obukhov, 1971). In coupled simulations, the ocean

11   temperature and salinity restoration options are turned off.

12   **2.2 Experiments design**

13   A set of numerical experiments were carried out with the coupled ocean-

14   atmosphere version of BESM-OA2.5, following the CMIP5 experiment design protocol

15   (Taylor et al., 2012), and shown schematically in Figure 1. Out of those experiments

16   listed below, only the Historical simulation is evaluated in this paper:

17   ●   Historical: the simulation runs over the period 1850−2005 (156 years), forced by

18   atmospheric equivalent CO_2 observed historical concentration (greenhouse gas

19   only) over this period, based on CMIP5 protocol.

20   ●   piControl: it runs for 700 years, forced by invariant pre-industrial atmospheric

21   CO_2 concentration level (280 ppmv).

22   ●   Abrupt 4×CO_2: it runs for 460 years, consisting of an abrupt quadruplication of

7

Geoscientific
Model Development
Discussions

1   the atmospheric CO_2 concentration level from the piControl simulation.

2   ● RCP4.5: it runs over the period 2006−2105 (100 years), forced by the time series

3   of greenhouse gases level projected by the Representative Concentration

4   Pathways 4.5 (RCP4.5), based on CMIP5 protocol. This simulation continues

5   the historical simulation throughout the 21th century, reaching the radiative

6   atmospheric forcing of 4.5 Wm^{-2} in 2100.

7   ● RCP8.5: same as the RCP4.5 simulation, but forced by the time series of

8   greenhouse gases level projected by the Representative Concentration Pathways

9   8.5 (RCP8.5), based on CMIP5 protocol; i.e., reaching the radiative atmospheric

10   forcing of 8.5 Wm^{-2} in 2100.

11

3. Methods and Data

13   To evaluate the outputs of the BESM-OA2.5 historical simulation, comparisons

14 are done against observed datasets and Reanalysis products. The atmospheric fields are

15 from the Twentieth-Century Reanalysis dataset version 2 (20CRv2; Compo et al., 2011)

16 with a global horizontal resolution of $2° \times 2°$ and 24 vertical levels

17 (https://www.esrl.noaa.gov/psd/data/gridded/data.20thC_ReanV2.html);   the

18 precipitation dataset is obtained from Global Precipitation Climatology Project version

19 2.2 Combined Precipitation Dataset (GPCP; Adler et al., 2003; Huffman et al., 2009)

20 with global horizontal resolution of $2.5° \times 2.5°$

21 (http://rda.ucar.edu/datasets/ds728.2/#!description); for comparison of the global

22 average air surface temperature, it is used the Hadley Centre-Climate Research Unit

23 Temperature Anomalies version 4 (HadCRUT4, Morice et al., 2012), globally averaged

1   air temperature anomaly at 2 meters time series

2   (https://crudata.uea.ac.uk/cru/data/temperature/); the cloud cover is compared to data

3   from The International Satellite Cloud Climatology Project (ISCCP D2; Rossow and

4   Schiffer, 1999) with global horizontal resolution of $2.5\,° \times 2.5\,°$

5   (https://isccp.giss.nasa.gov/products/onlineData.html); finally, for Sea Surface

6   Temperature (SST) comparisons it is used the Extended Reconstructed Sea Surface

7   Temperature version 4 (ERSSTv4, Huang et al., 2015) available on a $2\,° \times 2\,°$ grids

8   resolution (https://www.esrl.noaa.gov/psd/data/gridded/data.noaa.ersst.v4.html).

9   To identify the main modes of climate variability, all analyses presented in the

10   paper are done using detrended data sets anomalies. Detrended data sets are obtained by

11   removing the linear trend based on a least squares regression. Analysis using monthly

12   data sets, the annual cycle was removed by subtracting climatological monthly means

13   from the respective individual month. Prior to performing the analysis, the model's data

14   sets were interpolated to the grid resolution of the respective observation or Reanalysis

15   data sets used for comparison.

16   The Empirical Orthogonal Function analysis (EOF; Hannachi et al., 2007) is

17   used to analyze the capacity of the model in simulating major modes of climate

18   variability and compare them with observations. Prior to performing the EOF

19   calculations, the data were weighted by the square root of the cosine of latitude. The

20   results of the EOF maps are shown as the original data anomalies regressed onto the

21   normalized Principal Component (PC) time series, i.e. by the standard deviation.

22   In this paper, in order to evaluate the periodicity of the phenomena, it is applied

23   the power spectrum technique based on Fourier Analysis on the normalized time series,

1   in which the normalization is done by their long-term monthly standard deviation.

2   To have a better insight of BESM-OA2.5 performance of the global average

3   near-surface air temperature and on the average SST along both equatorial Pacific and

4   Atlantic, a comparison with 11 CMIP5 models is carried out. Since BESM-OA2.5

5   historical simulation is forced only by observed CO_2 equivalent concentration, for the

6   comparison it is chosen the historical simulation forced only by greenhouse gas

7   (historical GHG) shown in Table 1.

8

9   **4. Results**

10   **4.1 Mean Climate State**

11   In this section, the most important atmospheric and oceanic variables are

12   evaluated regarding their climatological fields, either globally or over regions in which

13   their representation are key elements of the climate system.

14   **4.1.1 Mean Surface Air Temperature**

15   The evolution of global surface air temperature throughout the industrial era is a

16   key element to analyze the long-term model behavior while being forced by the

17   observed conditions. The HadCRUT4 observation and BESM-OA2.5 time series of the

18   globally averaged air temperature anomaly at 2 meters are shown in Figure 2. The time

19   series are annual mean anomalies relative to the period 1850–1879. BESM-OA2.5

20   simulation of the global average surface air temperature evolution follows closely the

21   observed time series. However, since BESM-OA2.5 does not have the representation of

1   aerosols and consequently its cooling effects, the rate surface air warming should be

2   higher similarly to the remaining models (the grey shadow in Figure 2). In order to

3   compare BESM-OA2.5 with the selected CMIP5 models, the grey shadow represents

4   the spread of the minimum and the maximum values of anomalies at each year among

5   the 11 models (Table 1). In this comparison, it is used the historical GHG simulation, in

6   which the models are only forced by well-mixed greenhouse gases (mainly carbon

7   dioxide, methane, and nitrous oxides), without the cooling resulting from the direct and

8   indirect effects of aerosols, volcanos and effects of the land use change. Thus, the

9   CMIP5 models show a warmer tendency compared with the observations (see Jones et

10   al., 2013 for more details). Although BESM-OA2.5 has the same forcing conditions it

11   does not show the warming tendency of remaining models. The reason for the absence

12   of this warming tendency in the last decades of the 20th century is not clear. With

13   exception of GFDL-ESM2M (1861−2005) and HadGEM2-ES (1860−2005), all the

14   remaining CMIP5 models span their simulations throughout the period 1850−2005 and

15   their respective anomalies are from the period 1850−1879. For GFDL-ESM2M and

16   HadGEM2-ES, the anomalies are computed relative to the periods 1861−1890 and

17   1860−1889, respectively.

18   **4.1.2 Mean Precipitation**

19   One of the key points in evaluating a Climate Model is to gauge its ability to

20   simulate the hydrological cycle due to its importance to the energy balance of the

21   climate system. Figure 3 shows the spatial distribution of annual mean precipitation

22   biases for BESM-OA2.5. The bias is obtained through the difference with GPCP

23   dataset, in which the average values are computed over the periods 1971–2000 and

1   1979–2008, for BESM-OA2.5 and GPCP, respectively. BESM-OA2.5 is able to

2   reproduce global observed patterns of precipitation and indicates a slight improvement

3   in the global mean precipitation simulation compared with the previous version (BESM-

4   OA2.3). The spatial average biases are 0.3 mm day^{-1} and 0.5 mm day^{-1}, and the rmse are

5   1.4 mm day^{-1} and 1.7 mm day^{-1} for BESM-OA2.5 and BESM-OA2.3, respectively. The

6   improvements are particularly seen in the Pacific and Atlantic Ocean areas, where

7   BESM-OA2.5 reduces the positive bias that extends to subtropical southeast Pacific and

8   both north and south Atlantic subtropics observed in BESM-OA2.3 (see Fig. 6a of

9   Nobre et al., 2013). Despite these improvements, BESM-OA2.5 still generates a strong

10   negative bias over the Amazon region. The Indian subcontinent region also has a

11   significant negative bias and strong positive bias appears over the Indian Ocean and in

12   the South Pacific Convergence Zone (SPCZ). In order to draw an associated global

13   atmospheric circulation associated with the deficient precipitation over both the

14   Amazon and Indian regions, it is computed the global anomalies of the velocity

15   potential and the divergence of the wind at 200 hPa pressure level, and shown in Figure

16   4. The velocity potential and divergent wind anomalies are averaged over the period

17   1971−2000 for BESM-OA2.5 outputs (Fig. 4a), Reanalysis (Fig. 4b) and the difference

18   BESM-OA2.5 minus Reanalysis (Fig. 4c, 4d and 4e). Figure 4c shows anomalous

19   convergence over the Amazonian and Indian regions, resulting of the model's deficient

20   capacity for creating convection and consequently in generating precipitation. Figures

21   4d and 4e show the velocity potential and wind divergence separated by seasons. For

22   the Amazonian rainfall season, which occurs during MAM, it is possible to observe

23   anomalous convergence at high levels of the atmosphere (Fig 4d). The equivalent result

24   is observed for the Indian region for the JJA season (Fig. 4e).

1   Figure 5 shows zonally averaged precipitation during the four seasons. For this

2   comparison, results of BESM-OA2.3 used in Nobre et al. (2013) are also shown. Both

3   versions are able to reproduce the maximum peaks of precipitation in both tropical and

4   subtropical regions. BESM-OA2.5 shows a negative bias from around 40 ° latitude

5   poleward in both hemispheres. In the seasons DJF, JJA and SON, BESM-OA2.5 has a

6   positive bias on the peak of maximum precipitation corresponding to the ITCZ. In

7   MAM season the model still fails to perform the interhemispheric transition of the

8   ITCZ. However, the JJA season shows that BESM-OA2.5 is able to do the transition

9   completely, whilst BESM-OA2.3 shows a double ITCZ in JJA and SON seasons. The

10   double ITCZ problem is one of the most significant biases that persist in climate models

11   (e.g. Hwang and Frierson, 2013; Li and Xie, 2014; Tian, 2015). With the exception of

12   the MAM season, BESM-OA2.5 shows identical zonal precipitation to the observations,

13   although with a generally positive bias. It should be noted that BESM-OA2.5 has a

14   rapid precipitation decline at high latitudes. The model shows peaks of precipitation at

15   the mid-latitudes related to the storm tracks and less precipitation at the subtropics

16   compared to the GPCP dataset.

17   Figure 6 shows the general characteristics of cloudiness over the globe simulated

18   by the model. In particular, Figure 6a shows that the model underestimates cloudiness in

19   most part of the globe, with significant exceptions of the high latitudes in the boreal

20   hemisphere and in the southern subequatorial regions of the Pacific and Atlantic oceans

21   when compared to observations. Globally, BESM-OA2.5 has a cloudiness negative bias

22   of −13.9 % with a root-mean-square-error of 19.9 %. The periods used are 1971−2000

23   and 1984−2009 for BESM-OA2.5 and ISCCP, respectively. The model fails to generate

Geoscientific
Model Development
Discussions

1   clouds in the high latitudes of the austral hemisphere, as can be observed in Figure 6b,

2   where the percentage of cloud cover is negligible. The reason for such lack of simulated

3   cloudiness in this region is not clear yet. However, through the Figure 6b it is possible

4   to see the meridional variation of cloud cover simulated by the model is similar to the

5   observation.

6   **4.1.3 Zonal Atmospheric Mean State**

7   Figures 7 and 8 present the analysis of the zonally averaged vertical profiles of

8   air temperature and zonal wind for all seasons simulated by BESM-OA2.5 and the

9   respective bias relative to the 20CRv2 Reanalysis dataset, in which all data are time

10 averaged over the period 1971−2000. BESM-OA2.5 has a large positive air temperature

11 bias that appears above 250 hPa height (Fig. 7) in subpolar and polar regions in all

12 seasons. This result indicates that the model warms abnormally in the tropopause and

13 the lower stratosphere in polar regions. The warm bias is stronger in DJF and MAM

14 seasons over the northern polar region, reaching a maximum bias of 20 ℃ in the DJF

15 season. In the lower and middle troposphere, the model shows a negative temperature

16 bias, which is stronger in the lower troposphere over the polar region in the respective

17 winter-spring seasons in both hemispheres, i.e. DJF and MAM over the North Pole, and

18 JJA and SON over the South Pole. This negative bias reaches its maximum of −10 ℃

19 over the South Pole in SON. This negative bias over the troposphere has already been

20 reported to occur in many CMIP5 models (see Charlton-Perez et al., 2013; Tian et al.,

21 2013).

22 Concerning to the zonal wind, BESM-OA2.5 simulates a much weaker wind

23 speed at the tropopause and stratosphere over the boreal hemisphere, mainly in the DJF

1   season, which has a maximum negative bias of -26 m s^{-1} at $50-30$ hPa (Fig. 8a). The

2   tropospheric jets and their seasonal migration are reasonably well simulated, although

3   the eastward wind is stronger at subtropics with the maximum positive bias of 12 m s^{-1}

4   occurring at $300-100$ hPa in the MAM season.

5   **4.1.4 Mean Sea Surface Temperature**

6   The global distribution and the range values of the sea surface temperature

7   (SST) are important characteristics of the mean climate state. Figure 9 shows the spatial

8   map of the annual mean SST bias for BESM-OA2.5 relative to the ERSSTv4 dataset.

9   BESM-OA2.5 has a warm SST bias which spreads throughout all oceans, contrasting

10 with the negative biases which most of the CMIP5 models show over the North Pacific

11 and North Atlantic oceans (see Wang et al., 2014). Such a bias does not appear in the

12 tropical and subtropical regions in the BESM-OA2.3 simulation (Fig. 5a of Nobre et al.,

13 2013), where there are cold SST biases. The spatial average biases are 1.5 ℃ and 0.9

14 ℃, and the rmse are 1.9 ℃ and 2.1 ℃ for BESM-OA2.5 and BESM-OA2.3,

15 respectively. A notable feature of BESM-OA2.5 is its strong warm SST bias in the

16 North Pacific and in the Californian coast, and south of Greenland. The model still

17 overestimates SSTs in the major eastern coastal upwelling regions. Such a feature is a

18 systematic error observed in different state-of-the-art models, in which the causes can

19 be related to a simulation of a weaker than observed alongshore winds which leads to an

20 underrepresentation of upwelling and alongshore currents (e.g. Humboldt, California

21 and Benguela Currents), and/or the under predicted effects of shortwave radiation due to

22 deficient simulation of stratocumulus clouds over cold waters (see Richter, 2015).

23 Nevertheless, the bias is negligible over the north equatorial Pacific and in large parts of

1   tropical western Atlantic.

2   Figure 10a shows the mean SST along equatorial Pacific for BESM-OA2.5 and

3   ERSSTv4, averaged over the period 1971−2000. The equatorial region is defined over

4   the region between the latitudes 2 °S and 2 °N. The model simulates a warmer mean

5   SST over the western and extreme eastern parts of the equatorial Pacific Ocean. This

6   positive bias is most notable in the western part, where it is about 1.5−2 °C warmer than

7   observations and is warmer than the CMIP5 models (shown by the shaded grey area in

8   Figure 10a). But for the extreme eastern part of the basin, the model has a lower bias

9   compared with the CMIP5 models. For most of the central Pacific Ocean, the model has

10   a very good representation of the SST, with a RMSE of 0.14 °C between 160 °E and

11   120 °W. The annual cycle of the equatorial Pacific SST anomalies for BESM-OA2.5

12   and ERSSTv4 are shown in figure 10b and c, respectively. BESM-OA2.5 simulates

13   reasonably well the marked annual cycle which occurs on the eastern Pacific, although

14   the negative SST anomalies between July and December are up to 1 °C colder than

15   observations. The propagation of the SST anomaly patterns from the eastern to the

16   western part of the Pacific Ocean that occurs throughout the year is not well captured by

17   the model. BESM-OA2.5 shows an annual cycle in the western part of the Pacific

18   Ocean, where observations show a semiannual pattern of SST anomalies. The same

19   methodology is used for the tropical Atlantic. Figure 11a shows that in the Atlantic

20   basin there is a significant bias of ~3 °C in the eastern part of the basin. This bias starts

21   in the central Atlantic and it is higher than the CMIP5 models (shown by the shaded

22   grey area in Figure 11a). However, it should be noted that the CMIP5 models also have

23   a warm bias in the eastern part of the tropical Atlantic, which is a problem discussed in

24   previous studies (e.g. Richter et al., 2014 and references therein). Although this warm

1   bias, the tropical Atlantic seasonal SST variation is well simulated by BESM-OA2.5 in

2   particular on the eastern side of the basin, as it can be seen in Figures 11b and c.

3   **4.1.5 Atlantic Meridional Ocean Circulation**

4   The meridional overturning circulation (MOC) plays an important role in

5   transporting heat from the tropics to higher latitudes of both hemispheres. This is

6   particularly important in the North Atlantic, where the Atlantic Meridional Overturning

7   Circulation (AMOC) has a profound impact on the climate of the surrounding

8   continents (see Buckley and Marshall, 2015). The AMOC in the BESM-OA2.5

9   historical experiment has the typical structure described in Lumpkin and Speer (2007),

10 with the main layers well depicted in the appropriated depths (Figure 12a). The annual

11 mean maximum AMOC strength simulated by BESM-OA2.5 is about 15 Sv (1 Sv $\equiv 10^6$

12 $m^3 \ s^{-1}$) between 25 ºN and 30 ºN at about 850 m depth (see Figure 12a). This maximum

13 value is within the 17.2 ± 4.6 Sv mean strength (with a 10 day filtered root mean square

14 variability of 4.6 Sv) observed by the project RAPID at 26.5 $^\circ$ N (McCarthy et al.,

15 2015). It is also in the range of maximum volume transport strength simulated by the

16 state-of-the-art models of the CMIP5 (Weaver et al., 2012; Cheng et al., 2013). Figure

17 12b shows the maximum annual mean AMOC strength time series for the historical

18 period at the 30 $^\circ$ N. The same figure also plots the AMOC maximum volume transport

19 strength measured by the Rapid project over the period April/2004 to October/2015

20 (http://www.rapid.ac.uk/rapidmoc/rapid_data/datadl.php).

21   Averaging the maximum AMOC strength over the first and the last 30 years of

22 the time series, i.e. over the periods 1850−1879 and 1976−2005 respectively, the result

23 shows a decrease of 11.2 %, from 16.9 Sv to 15.1 Sv in each period, respectively.

1   Modeling results indicate that the AMOC has a multidecadal cycle, however the power

2   spectrum of its strength time series do not show a multidecadal oscillation (not shown).

3   The standard deviation of the detrended maximum AMOC strength time series is 1.4

4   Sv.

5

6   **4.2 Climate Variability**

7   In this section, we evaluate the most prominent global climate variability

8   patterns. This allows us to infer the ability of the model in simulating atmospheric

9   internal and ocean-atmosphere coupled variabilities in the climate system correctly.

10 **4.2.1 Tropical Variability**

11 **4.2.1.1 El Niño-Southern Oscillation**

12   The El Niño-Southern Oscillation (ENSO) in the equatorial Pacific Ocean is one

13 of the most prominent climate variability phenomena at interannual time scales

14 (Dijkstra, 2006), with strong impacts on regions surrounding the Indian and Pacific

15 Oceans and regions that are influenced by its teleconnections (see McPhaden et al.,

16 2006 and references therein). There are many methods to evaluate the ENSO variability.

17 In the present study, it is applied the EOF to detrended monthly SST anomalies over the

18 tropical Pacific ocean (30º S−30º N; 240º−70º W) for the period 1950−2005 for both

19 BESM-OA2.5 simulations and ERSSTv4 data. Figures 13a and b show the leading EOF

20 patterns associated with the El Niño/La Niña variability. The model simulates the El

21 Niño/La Niña variability deficiently, with lower amplitude of SST variability and the

22 center of maxima variability confined to the eastward part of the basin. The model's

1   leading EOF explains 17.9 % of the total variance, substantially less than the 45 %

2   explained by observations. The lower amplitude of the simulated El Niño/La Niña can

3   be verified in the power spectrum of the leading Principal Component (PC) shown in

4   Figure 13. Even though the simulation shows two significant peaks between 2−4 years

5   cycle (Fig. 13c), which is within the range of the period cycle given by the leading PC

6   of observations (3−7 years cycle; figure 13d), the amplitude of the simulated variance is

7   lower than that of observations.

8   Figure 14 shows the spatial correlation between detrended monthly anomalies of

9   the Niño-3 index (defined inside the black rectangle area, bounded by 5° S−5° N,

10   90°−150° W) and detrended monthly anomalies of global SST computed for BESM-

11   OA2.5 and ERSSTv4 over the period 1900−2005. The model has not a strong

12   correlation at grid points inside the Niño-3 area, which is a signal that the El Niño/La

13   Niña spatial pattern is weakly simulated. The horseshoe pattern of negative correlation

14   observed in the Pacific ocean is also weakly simulated by the model, particularly in the

15   westward equatorial part. The positive correlation of observed SST over the Indian

16   ocean and Niño-3 index is absent in the model's simulation. It is worth mentioning that

17   the model simulates the observed correlation pattern of SST anomalies over the Atlantic

18   Ocean with Ninõ-3 index, although it is not so robust (Figure 14).

19   **4.2.1.2 Atlantic Meridional Mode**

20   The leading modes of coupled ocean-atmosphere variability over the Tropical

21   Atlantic ocean are the zonal mode, also referred as equatorial mode (Zebiak, 1993; Lutz

22   et al., 2015), and the meridional mode, also referred as the interhemispheric mode

23   (Nobre and Shukla, 1996). The first is an ENSO-like phenomenon that emerges in the

1   Gulf of Guinea mainly in the boreal summer and has a strong impact on West African

2   precipitation (Zebiak, 1993; Lutz et al., 2015). The second is characterized by a cross-

3   equatorial SST gradient associated with a meridional wind stress toward the warmer

4   SST anomalies. The maxima amplitude of the meridional mode occurs during the boreal

5   spring, influencing the precipitation in Northeast Brazil and West Africa (Nobre and

6   Shukla, 1996; Chang et al., 1997; Chiang and Vimont, 2004). The Atlantic Meridional

7   Mode (AMM) has an interannual and decadal temporal scale of variability and is a

8   result of a thermodynamic coupling between the wind speed, the sea surface

9   evaporation induced by the wind stress, and the SST, mechanism known as Wind-

10 Evaporation-SST feedback (WES feedback, Xie and Philander, 1994; Chang et al.,

11 1997; Xie, 1999). To evaluate the AMM simulations, a joint EOF of SST and wind

12 stress (Taux and Tauy) fields analysis is computed, as such a variability is the response

13 of a coupled ocean-atmospheric system. Figure 15 shows the AMM simulated by

14 BESM-OA2.5, and obtained by observed data. The AMM pattern simulated by the

15 model is similar to obtained from observations, regardless of the weaker gradient pole at

16 the South Atlantic. Nevertheless, the explained variance by the model is very close to

17 the observed one, being respectively, 10.7 % and 11.8 %. The patterns shown in Figure

18 15 are defined as a positive phase of the AMM, with the inter-hemisphere cross-

19 equatorial wind from south to north, and with corresponding negative SST anomalies

20 over the southern pole and positive SST anomalies over the northern pole (the negative

21 phase of AMM is the reverse pattern). Over the second half of the 20th century, the

22 AMM shows a predominant decadal periodicity of 11−13 years. Figures 15c and d show

23 the power spectrum of the PC of the AMM patterns simulated by the model and from

24 the observation, respectively. It is possible to see that the pattern simulated by BESM-

1 OA2.5 shows, similarly to the observed one, a predominant periodicity at decadal

2 timescales.

3 **4.2.1.3 South Atlantic Convergence Zone**

4   The South Atlantic Convergence Zone (SACZ) is characterized by an intense

5 NW-SE oriented cloud band that extends from the Amazon Basin to the South Atlantic

6 subtropics, mainly during austral summer (Nogués-Paegle and Mo, 1997; Carvalho et

7 al., 2004; de Oliveira Vieira et al., 2013). The formation of the SACZ has a strong

8 influence on the precipitation over southeast South America and is considered, together

9 with the convection activity over the Amazon Basin, the main component of the South

10 American Monsoon System (Jones and Carvalho, 2002). The southern part of the SACZ

11 usually lies over cooler SST (Grimm, 2003; Robertson and Mechoso, 2000). Chaves

12 and Nobre (2004) suggests that the formation of SACZ over the ocean tend to block the

13 solar radiation by clouds, cooling the SST beneath. AGCM are not able to simulate the

14 precipitation over cooler SST caused by SACZ (Marengo et al., 2003; Nobre et al.,

15 2006; Nobre et al., 2012), since such models tend to increase the precipitation over

16 warmer SST, as an hydrostatic response. Nobre et al. (2012) has shown that coupled

17 AOGCMs are able to simulate the SACZ formation over colder SST anomalies, as this

18 class of models englobes the atmosphere-ocean surface thermodynamic coupling.

19 Following Nobre et al. (2012), a correlation between seasonal precipitation and SST

20 anomalies for the austral summer (DJF) over the tropical South Atlantic (40º S−10º N;

21 70º W−20º E) over the period 1979−2010 for observations and for the period

22 1971−2002 for the model, so 32 years are used. Figure 16 shows the rainfall-SST

23 anomaly correlation maps for both BESM-OA2.5 and observations. BESM-OA2.5 are

Geoscientific
Model Development
Discussions

1   able to simulate an inverse correlation between precipitation and SST in the southeast of

2   Brazil (near 20 °S), suggesting the capacity of simulating precipitation over cooler SST,

3   a feature related to the formation of SACZ (that tends to cooler the SST). Its noteworthy

4   in Figure 16 that BESM-OA2.5 is capable to generate both positive and negative SSTA-

5   rainfall correlations over the equatorial Atlantic (positive, thermally direct driven

6   circulation over the equatorial region and negative, thermally indirect driven

7   atmospheric circulation over the SW tropical Atlantic, Figure 16a), a feature also

8   present in the observation correlation map of Figure 16b.

9   **4.2.2 Extratropical Variability**

10 **4.2.2.1 North Atlantic Oscillation**

11   The North Atlantic Oscillation (NAO) is a major atmospheric variability pattern

12 occurring in the North Atlantic, which is characterized by the oscillation of the

13 difference on the sea level pressure (SLP) between Iceland and Portugal (Wanner et al.,

14 2001; Hurrel et al., 2003). NAO has a great impact in the Euro-Atlantic region (Hurrell

15 et al., 2003; Hurrell and Deser, 2009), with the notable work of Namias (1972) relating

16 droughts over the Northeast Brazil to NAO variations. Recent studies also show its

17 teleconnections to the East Asia (e.g. Yu and Zhou, 2004; Wu et al., 2012). The NAO's

18 influence on a rapid climate change in the Northern Hemisphere has been highlighted in

19 (Delworth et al., 2016), which increases the importance of its correct simulation. Since

20 NAO's largest amplitude of variation occurs mainly during the boreal winter, the

21 analysis here is centered on this season. The period used to perform the analyses is

22 1950−2005. The leading EOF of the SLP averaged for boreal winter season (DJF) in the

23 Euro-Atlantic region shows that the NAO is well simulated by BESM-OA2.5 (Fig. 17a),

Geoscientific
Model Development
Discussions

1   simulating the NAO dipole centers and their amplitudes very similar to the observed

2   pattern (Fig. 17b). The variances explained by the leading EOF are also similar, 50.2 %

3   and 44 % for BESM-OA2.5 and Reanalysis, respectively. The spectral analysis of the

4   leading PCs shows that BESM-OA2.5 captures the ~2.5 years cycle on the time

5   variability but fails to capture the ~8 years cycle (Fig. 17c and d). It is interesting to

6   note that BESM-OA2.5 simulates a NAO spatial pattern, without capturing its low-

7   frequency variability. By analyzing the NAO variability, we consider that it is not

8   necessary to analyze the Northern Annular Mode (NAM), since both are manifestation

9   of same mode of variability (Hurrell and Deser, 2009).

10   **4.2.1.2 Pacific-North America Pattern**

11   Jointly, the NAO and the Pacific-North American pattern (PNA) are the

12   dominant atmospheric internal modes over the boreal hemisphere. The PNA is

13   characterized by four centers of high pressure anomalies in the North Pacific and North

14   America, respectively; over Hawaii, to the south of the Aleutian Islands, in the

15   intermountain region of North America, and in the Gulf Coast region of the U.S.A.,

16   representing the centers of action of a stationary wave train extending from the tropical

17   Pacific into North America (Wallace and Gutzler, 1981). It exerts a significant influence

18   on surface temperature and precipitation over North America (Leathers et al., 1991).

19   Some studies have shown that, although the PNA is an internal atmospheric variability

20   phenomena, it is influenced by other climate variabilities, as the ENSO and the Pacific

21   Decadal Oscillation (PDO) (see Straus and Shukla, 2002; Yu and Zwiers, 2007).

22   Similar to NAO, the PNA has its largest variation of amplitude during the boreal

23   winter; therefore, the present analysis is performed for this season. Following Wallace

1   and Gutzler (1981), we construct one-point correlation maps for BESM-OA2.5 and

2   20CRv2 Reanalysis in order to evaluate the capacity of the model to reproduce the PNA

3   pattern. The one-point correlation maps correlate 500 hPa geopotential height at the

4   reference point (45º N, 165º W) with all the other grid points of the map domain (0º−80º

5   N; 240º−70º W). The time series used to perform the correlations are averaged boreal

6   winter seasonal (DJF) dataset over the period 1950−2005. The time series are departed

7   from their long-term mean and normalized at each grid point prior the correlation

8   computation. Figure 18 shows the one-point correlation maps for BESM-OA2.5 (Fig.

9   18a) and 20CRv2 (Fig. 18b). In this figure, it is possible to check the four centers of

10 action simulated by the model, which shows a stronger correlation between the four

11 high pressure centers when compared with reanalysis correlation maps in Figure 18b.

12 **4.2.1.2 Pacific-South America Patterns**

13   The second and third EOF of 500 hPa geopotential height over the Southern

14 Hemisphere (20º−90º S) present a notable resemblance to the Pacific-South America

15 (PSA) teleconnection pattern (Ghil and Mo, 1991). PSA patterns are stationary Rossby

16 wave trains extending from central Pacific to Argentina, in which the PSA1 (EOF2) is a

17 response to ENSO and the PSA2 (EOF3) is associated to the quasi-biennial component

18 of ENSO (Karoly, 1989; Mo and Peagle, 2001). These patterns have a significant

19 impact on rainfall anomalies over South America (Mo and Peagle, 2001). Figure 19

20 shows the PSA patterns both simulated by BESM-OA2.5 and from Reanalysis. As the

21 explained variance of EOF2 and EOF3 are close, the EOFs seem to degenerate for both

22 Reanalysis and model simulation. In order to relax the orthogonality constraint, it is

23 performed a rotated EOF (REOF) retaining the first 10 modes. The REOF2 and REOF3

1   resemble the EOF2 and EOF3 respectively, implying that they are independent modes.

2   The PSA pattern is well simulated by BESM-OA2.5, although the model changes the

3   order of the EOF patterns. BESM-OA2.5 shows an anomaly south of South Africa (Fig

4   19c) that do not appear in the Reanalysis (Fig 19b). PSA patterns have significant

5   interannual and decadal variabilities (Zhang et al., 2016). PSA patterns simulated by

6   BESM-OA2.5 have only significant variability in the interannual scale, with absent

7   decadal variability (figure not shown).

8   **4.2.1.4 Southern Annular Mode**

9   The Southern Annular Mode (SAM) is the dominant atmospheric variability in

10   the Southern Hemisphere, occurring in the extra-tropics and in the high latitudes

11   (Kidson,1988). It is also referred to as Antarctic Oscillation (AAO; Gong and Wang,

12   1999). SAM variability is characterized by anomalies variation in the polar low-

13   pressure and in the surrounded zonally high-pressure belt. It can be captured through the

14   first EOF applied to different atmospheric variables, as the sea level pressure, different

15   geopotential height levels or the surface air temperature (Kidson, 1988; Rogers and van

16   Loon, 1982; Thompson and Wallace, 2000). To evaluate the capacity of BESM-OA2.5

17   to simulate this atmospheric mode of variability, EOF analysis is applied to the monthly

18   mean 500 hPa geopotential height field from 20º S to 90º S, over the period 1950−2005,

19   for both model and Reanalysis. The SAM pattern simulated by BESM-OA2.5 resembles

20   very well the observed pattern, with the mid-latitude 500 hPa geopotential height

21   variation centers depicted in the same longitudes as observations, but with differences in

22   the amplitude values (Fig. 20). However, the explained variance is higher compared

23   with observation. The explained variances of BESM-OA2.5 and 20CRv2 are 34.1 %

Geoscientific
Model Development
Discussions

1 and 21.0 %, respectively. The SAM is a quasi-decadal mode of variability (see Yuan

2 and Yonekura, 2011), however the BESM-OA2.5 power spectrum reveals a SAM with

3 a markedly interannual variability, without the peak between 8 and 16 years as obtained

4 in the Reanalysis (figure not shown).

5 **4.2.1.5 Pacific Decadal Oscillation**

6 Observed SST anomalies over the North Pacific have shown an oscillatory

7 pattern in the central and western parts in relation to the tropical part and along the

8 North American west coast. This oscillatory shift of SST anomalies with interdecadal

9 periodicity was termed Pacific Decadal Oscillation (PDO) and it is defined as the

10 leading EOF of the monthly SST anomalies over North Pacific (Mantua et al., 1997).

11 The positive phase of PDO is defined when positive SST anomalies predominate over

12 the central and western parts of North Pacific, and negative SST anomalies predominate

13 over the Tropical Pacific and along the North American west coast; being the negative

14 phase the reverse pattern. Many studies have connected the PDO with variations on

15 precipitation regimes in different regions around the world, as South China monsoon

16 (e.g. Wu and Mao, 2016), Indian monsoon (e.g. Krishnamurthy and Krishnamurthy,

17 2016) and together with ENSO in the precipitation regime in North America (see Hu

18 and Huang, 2009). There are different mechanisms that modulate PDO, in which one of

19 them is the response of the Northern Pacific SST to the ENSO variability via the

20 "atmospheric bridge" (for a detailed review, see Newman et al., 2016).

21 Following the definition (Mantua et al., 1997), the spatial pattern of PDO is

22 obtained by regressing the SST anomalies onto the leading normalized PC time series,

23 shown in Figure 21 which in this case is showing the positive phase of the PDO. The

26

1 EOF is applied to monthly SST anomalies over North Pacific (20º−60º N; 240º−110º

2 W) over the period 1900−2005. BESM-OA2.5 is not capable of reproducing this pattern

3 by the leading EOF. The PDO pattern only appears on the second EOF (Fig. 21b), with

4 the explained variance of 14.0 % against 20.5 % of observations. Although the EOF2

5 resembles the PDO mode, the tropical part has a weaker variation than the observation.

6 The reason of incapacity of the model in reproducing the PDO as the leading mode of

7 variability is probably due to the model's simulation of weaker ENSO variability, both

8 in spatial and temporal scales. These deficiencies may impact the mechanisms that

9 reproduce the PDO, mainly via the "atmospheric bridge" as referred earlier. Figures 22a

10 and b show the normalized PC2 and PC1 time series of BESM-OA2.5 and ERSSTv4,

11 respectively. It is possible to note that both time series present a multidecadal

12 periodicity, but in different time scales as it is confirmed by the power spectrum (Fig.

13 22c and d). The power spectrum shows that both time series present interannual

14 periodicity (~5-6 years), with BESM-OA2.5 multidecadal variability strongest spectrum

15 around 15 years, a higher frequency compared with observation (~22 and ~40-45 years).

16

5. Summary

18 The capacity of Earth Systems Models to project a future climate under the

19 conditions given by future scenarios of atmospheric greenhouse gas concentrations can

20 be assessed by how accurate these models are able to reproduce observed climate

21 features. Therefore, the evaluation of how these models perform for the historical period

22 when there are observations to compare with model's calculations represents a key part

23 of the Earth System modelling. In this study, BESM-OA2.5 historical simulation is

1   evaluated for the period 1850−2005 following the CMIP5 protocol (Taylor et al., 2012)

2   with focus on simulations of its mean climate and key large-scale modes of climate

3   variability.

4   BESM-OA2.5 is an updated version of BESM-OA2.3 (Nobre et al. 2013;

5   Giarolla et al. 2015) regarding the atmospheric model, which consists in the new

6   Brazilian Global Atmospheric Model (BAM; Figueroa et al., 2016). This new version

7   allowed to alleviate a mean global bias of energy balance at the top of the atmosphere of

8   -20 Wm^{-2} to 2 Wm^{-2}.Moreover, systematic errors were reduced in wind, humidity and

9   temperature in the surface layer over oceanic regions by the inclusion formulations

10   presented by Jiménez et al. (2012).

11   The analysis of the mean climate shows that the model is able to simulate the

12   general mean climate state. Nevertheless, some significant biases appear at the

13   simulation, as a double ITCZ over the Pacific and Atlantic Oceans, some notable

14   regional biases in the precipitation field (e.g., over the Amazon and Indian regions) and

15   in the SST field (e.g., south of Greenland). Yet, the model has shown an improvement

16   in simulating the ITCZ and a reduction in the global precipitation RMSE compared with

17   BESM-OA version 2.3. BESM-OA2.5 shows an almost globally positive SST bias,

18   which did not occur in version 2.3, however the SST RMSE was slightly reduced in the

19   newer version of the model.

20   The most relevant climate patterns on interannual to decadal time scales

21   simulated by BESM-OA2.5 are compared with the ones obtained from observations and

22   Reanalysis. Over the Pacific, the ENSO is simulated with lower amplitude of variability

23   than the observations and such weak ENSO seems to impact other Pacific variability

1   patterns such as the PDO. Conversely, the major phenomena on the Atlantic basin are

2   well represented in BESM-OA2.5 simulations. This is the case for the Tropical Atlantic

3   mode of interhemispheric variability (AMM) that is very well simulated by the model in

4   term of the spatial pattern and temporal variability. It is worth to note that this mode is

5   considered poorly simulated by the models used in the Intergovernmental Panel on

6   Climate Change (IPCC) fifth assessment report (AR5) (Flato et al., 2013). It is also

7   relevant to highlight BESM-OA2.5 ability to represent the enhanced rainfall over cooler

8   waters over the SW Tropical Atlantic, associated with the South Atlantic Convergence

9   Zone (SACZ). The capacity of the model in simulating the AMM and SACZ is an

10 important result since one of the main aims is the representation of modes that directly

11 impacts the precipitation over South America. The AMOC reproduced by BESM-

12 OA2.5 has the meridional overturning structure comparable with the ensemble AMOC

13 simulated by the CMIP5's models. BESM's maximum AMOC strength average value is

14 slighter lower than the average value that has been observed by the project RAPID, but

15 well within the range of mean square root variability that is observed. Although the

16 averaged maximum strength AMOC simulated by the CMIP5 models is within the

17 mean range square root variability that is observed, most models tend to simulate strong

18 AMOC, with a maximum strength above 20 Sv, and out of the range (Zhang and Wang,

19 2013). The NAO atmospheric variability, which is well simulated by the CMIP5 models

20 (Ning and Bradley, 2016) is also very well simulated by BESM-OA2.5. In the extra-

21 tropics, BESM-OA2.5 is capable to reproduce fairly well majors variabilities in both

22 Hemispheres, as the PNA, PSA, and the SAM teleconnections patterns, comparable to

23 CMIP5 models that reproduce the PNA (Ning and Bradley, 2016) and the SAM (Zheng

24 et al. 2013).

1   Similarly to Nobre et al. (2013), this study aims to evaluate the BESM-OA2.5

2 by comparing the most important features of the climate system simulated by the model

3 with observations and Reanalysis. The next version of the model (BESM-OA2.8) is

4 already under development. In this new version, the MOM4p1 ocean model has been

5 replaced by the MOM5. Regarding the atmospheric model, new developments have

6 been carried out to improve BAM's capacity, being the most important the inclusion of

7 a scheme of humidity in the planetary boundary layer, a new dynamic core and new

8 cloud cover scheme (Figueroa et al., 2016). This new version of BESM carries the

9 challenges of improving the simulation of the precipitation, in particular to alleviate the

10 deficit over the Amazon. The ENSO is the large-scale phenomenon that will receive a

11 scrutiny in order to understand the reasons for a weak variability. The other feature of

12 the model is the weaker warming under the CO_2 equivalent only forcing, relative to

13 other CMIP5 that do not consider the direct and indirect effects of atmospheric aerosols.

14 In the future, a study comparing the versions 2.5 and 2.8 of the BESM-OA is aimed in

15 order to fully report the advances of the modeling work developed in the last couple

16 years. Such a study will give a broader perspective of the technical challenges overcome

17 throughout this project and assess the improvements achieved in each version of the

18 model in simulating the climate system.

19

20 **Code and data availability**

21 The BESM-OA2.5 source code is freely available after signature of a license agreement.

22 Please contact Paulo Nobre to obtain the source code and data of BESM-OA2.5.

Geoscientific
Model Development
Discussions

1

Competing interests

There are no competing interests of which the authors are aware.

Acknowledgements

10

References

Adler, R. F., Huffman, G. J., Chang, A., Ferraro, R., Xie, P.-P., Janowiak, J., Rudolf, B., Schneider, U., Curtis, S., Bolvin, D., Gruber, A., Susskind, J., Arkin, P. and Nelkin, E.: The Version-2 Global Precipitation Climatology Project (GPCP) Monthly Precipitation Analysis (1979–Present), J. Hydrometeorol., 4(6), 1147–1167, doi:10.1175/1525-7541(2003)004<1147:TVGPCP>2.0.CO;2, 2003.

Anthes, R. A.: A Cumulus Parameterization Scheme Utilizing a One-Dimensional Cloud Model, Mon. Weather Rev., 105(3), 270–286, doi:10.1175/1520-0493(1977)105<0270:ACPSUA>2.0.CO;2, 1977.

Arakawa, A. and Schubert, W. H.: Interaction of a Cumulus Cloud Ensemble with the Large-Scale Environment, Part I, J. Atmos. Sci., 31(3), 674–701, doi:10.1175/1520-0469(1974)031<0674:IOACCE>2.0.CO;2, 1974.

Bottino, M. J., and Nobre, P.: Impacts of cloud cover schemes on the Atlantic climate in the Brazilian Earth System Model – BESM-OA2.3. (Submitted to Climate Dynamics).

Buckley, M. W. and Marshall, J.: Observations, inferences, and mechanisms of the Atlantic Meridional Overturning Circulation: A review, Rev. Geophys., 54, 5–63, doi:10.1002/2015RG000493.Received, 2015.

Capistrano, V., Nobre, P., Tedeschi, R., Silva, J., Bottino, M.,Baptista Jr., M., Menezes Neto, O., Figueroa, S. N., Bonatti, J.P., Kubota, P., Fernandez J., Giarolla, E., Vial, J., Nobre, C. A.: Overview of climate change in the BESM-OA2.5 climate model. (Submitted to Journal of Climate).

Carvalho, L. M. V, Jones, C. and Liebmann, B.: The South Atlantic convergence zone: Intensity, form, persistence, and relationships with intraseasonal to interannual activity and extreme rainfall, J. Clim., 17(1), 88–108, doi:10.1175/1520-0442(2004)017<0088:TSACZI>2.0.CO;2, 2004.

Geoscientific
Model Development
Discussions

Open Access

EGU

1 Chang, P., Ki, L. and Li, H.: A decadal climate variation in the tropical Atlantic Ocean
2   from thermodynamic air-sea interactions, Nature, 385(6), 516–518,
3   1997.

4 Charlton-Perez, A. J., Baldwin, M. P., Birner, T., Black, R. X., Butler, A. H., Calvo, N.,
5   Davis, N. A., Gerber, E. P., Gillett, N., Hardiman, S., Kim, J., Krüger, K., Lee,
6   Y. Y., Manzini, E., McDaniel, B. A., Polvani, L., Reichler, T., Shaw, T. A.,
7   Sigmond, M., Son, S. W., Toohey, M., Wilcox, L., Yoden, S., Christiansen, B.,
8   Lott, F., Shindell, D., Yukimoto, S. and Watanabe, S.: On the lack of
9   stratospheric dynamical variability in low-top versions of the CMIP5 models, J.
10   Geophys. Res. Atmos., 118(6), 2494–2505, doi:10.1002/jgrd.50125, 2013.

11 Chaves, R. R. and Nobre, P.: Interactions between sea surface temperature over the
12   South Atlantic Ocean and the South Atlantic Convergence Zone, Geophys. Res.
13   Lett., 31(3), 1–4, doi:10.1029/2003GL018647, 2004.

14 Cheng, W., Chiang, J. C. H. and Zhang, D.: Atlantic meridional overturning circulation
15   (AMOC) in CMIP5 Models: RCP and historical simulations, J. Clim., 26(18),
16   7187–7197, doi:10.1175/JCLI-D-12-00496.1, 2013.

17 Chiang, J. C. H. and Vimont, D. J.: Analogous Pacific and Atlantic Meridional Modes
18   of Tropical Atmosphere – Ocean Variability, J. Clim., 17, 4143–4158,
19   doi:10.1175/JCLI4953.1, 2004.

20 Chou, M.-D. and Suarez, M. J.: A solar radiation parame- terization (CLIRAD-SW) for
21   atmospheric studies. NASA Tech. Memo NASA/TM-1999-104606, 40 pp.,
22   1999.

23 Chou, S. C., Lyra, A., Mourão, C., Dereczynski, C., Pilotto, I., Gomes, J., Bustamante,
24   J., Tavares, P., Silva, A., Rodrigues, D., Campos, D., Chagas, D., Sueiro, G.,
25   Siqueira, G., Nobre, P. and Marengo, J.: Evaluation of the Eta Simulations
26   Nested in Three Global Climate Models, Am. J. Clim. Chang., 3(5), 438–454,
27   doi:10.4236/ajcc.2014.35039, 2014.

28

Geoscientific
Model Development
Discussions

1   Compo, G. P., Whitaker, J. S., Sardeshmukh, P. D., Matsui, N., Allan, R. J., Yin, X.,
2   Gleason, B. E., Vose, R. S., Rutledge, G., Bessemoulin, P., BroNnimann, S.,
3   Brunet, M., Crouthamel, R. I., Grant, A. N., Groisman, P. Y., Jones, P. D., Kruk,
4   M. C., Kruger, A. C., Marshall, G. J., Maugeri, M., Mok, H. Y., Nordli, O.,
5   Ross, T. F., Trigo, R. M., Wang, X. L., Woodruff, S. D. and Worley, S. J.: The
6   Twentieth Century Reanalysis Project, Q. J. R. Meteorol. Soc., 137(654), 1–28,
7   doi:10.1002/qj.776, 2011.

8   Delworth, T. L. and Mann, M. E.: Observed and simulated multidecadal variability in
9   the   Northern   Hemisphere,   Clim.   Dyn.,   16(9),   661–676,
10   doi:10.1007/s003820000075, 2000.

11 Delworth, T. L., Zeng, F., Vecchi, G. A., Yang, X., Zhang, L. and Zhang, R.: The North
12   Atlantic Oscillation as a driver of rapid climate change in the Northern
13   Hemisphere, Nat. Geosci., 9(7), 509–512, doi:10.1038/ngeo2738, 2016.

14 Dijkstra, H. A.: The ENSO phenomenon: theory and mechanisms, Adv. Geosci., 6, 3–
15   15, doi:10.5194/adgeo-6-3-2006, 2006.

16 Enfield, D. B., Mestas-Nuñez, A. M. and Trimble, P. J.: The Atlantic multidecadal
17   oscillation and its relation to rainfall and river flows in the continental U.S,
18   Geophys. Res. Lett., 28(10), 2077–2080, doi:10.1029/2000GL012745, 2001.

19 Ferrier, B. S., Jin, Y., Lin, Y., Black, T., Rogers, E. and DiMego, G.: Implementation of
20   a 527 new grid-scale cloud and precipitation scheme in the NCEP Eta model.
21   Amer. Meteor. Soc., 280–283, 2002.

22 Figueroa, S. N., Bonatti, J. P., Kubota, P. Y., Grell, G. A., Morrison, H., Barros, S. R.
23   M., Fernandez, J. P. R., Ramirez, E., Capistrano, V. B., Alvim, D. S., Enoré, D.
24   P., Diniz, F. L. R., Barbosa, H. M. J., Mendes, C. L. and Panetta, J.: The
25   Brazilian Global Atmospheric Model (BAM): Performance for Tropical Rainfall
26   Forecasting and Sensitivity to Convective Scheme and Horizontal Resolution,
27   Weather Forecast., 31(5), 1547–1572, doi:10.1175/WAF-D-16-0062.1, 2016.

28 Flato, G. M.: Earth system models: An overview, Wiley Interdiscip. Rev. Clim. Chang.,

1   2(6), 783–800, doi:10.1002/wcc.148, 2011.

2   Flato, G., J. Marotzke, B. Abiodun, P. Braconnot, S.C. Chou, W. Collins, P. Cox, F.

3   Driouech, S. Emori, V. Eyring, C. Forest, P. Gleckler, E. Guilyardi, C. Jakob, V.

4   Kattsov, C. Reason and M. Rummukainen, 2013: Evaluation of Climate Models.

5   In: Climate Change 2013: The Physical Science Basis. Contribution of Working

6   Group I to the Fifth Assessment Report of the Intergovernmental Panel on

7   Climate Change [Stocker, T.F., D. Qin, G.-K. Plattner, M. Tignor, S.K. Allen, J.

8   Boschung, A. Nauels, Y. Xia, V. Bex and P.M. Midgley (eds.)]. Cambridge

9   University Press, Cambridge, United Kingdom and New York, NY, USA.

10   Ghil, M. and Mo, K.: Intraseasonal Oscillations in the Global Atmosphere. Part I:

11   Northern   Hemisphere   and   Tropics,   J.   Atmos.   Sci.,   48(5),   752–779,

12   doi:10.1175/1520-0469(1991)048<0752:IOITGA>2.0.CO;2, 1991.

13   Giarolla, E., Siqueira, L. S. P., Bottino, M. J., Malagutti, M., Capistrano, V. B. and

14   Nobre, P.: Equatorial Atlantic Ocean dynamics in a coupled ocean atmosphere

15   model simulation, Ocean Dyn., 65(6), 831–843, doi:10.1007/s10236-015-0836-

16   8, 2015.

17   Gong, D. and Wang, S.: Definition of Antarctic Oscillation Index, Geophys. Res. Lett.,

18   26(4), 459–462, doi:10.1029/1999GL900003, 1999.

19   Grell, Georg and Dévényi, D. A.: A generalized approach to parameterizing convection

20   combining ensemble and data assimilation techniques, Geophys. Res. Lett.,

21   29(14), 10–13, doi:10.1029/2002GL015311, 2002.

22   Griffies, S. M.: Elements of MOM4p1. NOAA/Geophysical Fluid Dynamics Laboratory

23   Ocean Group Tech. Rep. 6, 444 pp., 2009.

24   Grimm, A. M.: The El Niño impact on the summer monsoon in Brazil: Regional

25   processes versus remote influences, J. Clim., 16(2), 263–280, doi:10.1175/1520-

26   0442(2003)016<0263:TENIOT>2.0.CO;2, 2003.

27   Harshvardhan, Davies, R., Randall, D. A. and Corsetti, T. G.: A fast radiation

1   parameterization for atmospheric circulation models, J. Geophys. Res., 92(D1),
2   1009–1016, doi:10.1029/JD092iD01p01009, 1987.

3   Hu, Z. Z. and Huang, B.: Interferential impact of ENSO and PDO on dry and wet
4   conditions in the U.S. great plains, J. Clim., 22(22), 6047–6065,
5   doi:10.1175/2009JCLI2798.1, 2009.

6   Huang, B., Banzon, V. F., Freeman, E., Lawrimore, J., Liu, W., Peterson, T. C., Smith,
7   T. M., Thorne, P. W., Woodruff, S. D. and Zhang, H. M.: Extended
8   reconstructed sea surface temperature version 4 (ERSST.v4). Part I: Upgrades
9   and intercomparisons, J. Clim., 28(3), 911–930, doi:10.1175/JCLI-D-14-
10   00006.1, 2015.

11 Huffman, G. J., Adler, R. F., Bolvin, D. T. and Gu, G.: Improving the global
12   precipitation record: GPCP Version 2.1, Geophys. Res. Lett., 36(17), L17808,
13   doi:10.1029/2009GL040000, 2009.

14 Hurrell, J. W. and Deser, C.: North Atlantic climate variability: The role of the North
15   Atlantic   Oscillation,   J.   Mar.   Syst.,   78(1),   28–41,
16   doi:10.1016/j.jmarsys.2008.11.026, 2009.

17 Hurrell, J. W., Kushnir, Y., Otterson, G. and Visbeck, M.: An Overview of the North
18   Atlantic Oscillation, North Atl. Oscil. Clim. Significance Environ. Impact, 134,
19   263, doi:10.1029/GM134, 2003.

20 Hwang, Y.-T. and Frierson, D. M. W.: Link between the double-Intertropical
21   Convergence Zone problem and cloud biases over the Southern Ocean., Proc.
22   Natl. Acad. Sci. U. S. A., 110(13), 4935–40, doi:10.1073/pnas.1213302110,
23   2013.

24 Jiménez, P. A., Dudhia, J., González-Rouco, J. F., Navarro, J., Montávez, J. P. and
25   García-Bustamante, E.: A Revised Scheme for the WRF Surface Layer
26   Formulation, Mon. Weather Rev., 140(3), 898–918, doi:10.1175/MWR-D-11-
27   00056.1, 2012.

Geoscientific
Model Development
Discussions

1 Jones, C. and Carvalho, L. M. V: Active and break phases in the South American
2   monsoon system, J. Clim., 15(8), 905–914, doi:10.1175/1520-
3   0442(2002)015<0905:AABPIT>2.0.CO;2, 2002.

4 Karoly, D. J.: Southern Hemisphere Circulation Features Associated with El-Nino-
5   Southern Oscillation Events, J. Clim., 2, 1239–1252, doi: 10.1175/1520-
6   0442(1989)002<1239:SHCFAW>2.0.CO;2., 1989.

7 Kidson, J. W.: Interannual Variations in the Southern Hemisphere Circulation, J. Clim.,
8   1(12), 939–953, doi:10.1175/1520-0442(1988)001<1177:IVITSH>2.0.CO;2,
9   1988.

10 Krishnamurthy, L. and Krishnamurthy, V.: Indian monsoon' s relation with the decadal
11   part of PDO in observations and NCAR CCSM4, Int. J. Climatol.,
12   doi:10.1002/joc.4815, 2016.

13 Large, W. G. and Yeager, S. G.: The global climatology of an interannually varying air
14   - Sea flux data set, Clim. Dyn., 33(2–3), 341–364, doi:10.1007/s00382-008-
15   0441-3, 2009.

16 Leathers, D. J., Yarnal, B., Palecki, M. A., Leathers, D. J., Yarnal, B. and Palecki, M.
17   A.: The Pacific/North American Teleconnection Pattern and United States
18   Climate. Part I: Regional Temperature and Precipitation Associations, J. Clim.,
19   4(5), 517–528, doi:10.1175/1520-0442(1991)004<0517:TPATPA>2.0.CO;2,
20   1991.

21 Levitus, S.: Climatological Atlas of the World Ocean.NOAA Prof. Paper 13, 173 pp.
22   and 17 microfich, 1982.

23 Li, G. and Xie, S. P.: Tropical biases in CMIP5 multimodel ensemble: The excessive
24   equatorial pacific cold tongue and double ITCZ problems, J. Clim., 27(4), 1765–
25   1780, doi:10.1175/JCLI-D-13-00337.1, 2014.

26 Lu, R., Dong, B. and Ding, H.: Impact of the Atlantic Multidecadal Oscillation on the
27   Asian summer monsoon, Geophys, Res. Lett., 33, L24701, doi(24), 101029/,

Geoscientific
Model Development
Discussions

1   doi:10.1029/2006GL027655, 2006.

2   Lumpkin, R. and Speer, K.: Global Ocean Meridional Overturning, J. Phys. Oceanogr.,
3   37(10), 2550–2562, doi:10.1175/JPO3130.1, 2007.

4   Lutz, K., Jacobeit, J. and Rathmann, J.: Atlantic warm and cold water events and impact
5   on African west coast precipitation, Int. J. Climatol., 35(1), 128–141,
6   doi:10.1002/joc.3969, 2015.

7   Mantua, N. J., Hare, S. R., Zhang, Y., Wallace, J. M. and Francis, R. C.: A Pacific
8   Interdecadal Climate Oscillation with Impacts on Salmon Production, Bull. Am.
9   Meteorol. Soc., 78(6), 1069–1079, doi:10.1175/1520-
10   0477(1997)078<1069:APICOW>2.0.CO;2, 1997.

11   Marengo, J. A., Calvalcanti, I. F. A., Satyamurty, P., Trosnikov, I., Nobre, C. A.,
12   Bonatti, J. P., Camargo, H., Sampaio, G., Sanches, M. B., Manzi, A. O., Castro,
13   C. A. C., D'Almeida, C., Pezzi, L. P. and Candido, L.: Assessment of regional
14   seasonal rainfall predictability using the CPTEC/COLA atmospheric GCM,
15   Clim. Dyn., 21(5–6), 459–475, doi:10.1007/s00382-003-0346-0, 2003.

16   McCarthy, G. D., Smeed, D. A., Johns, W. E., Frajka-Williams, E., Moat, B. I., Rayner,
17   D., Baringer, M. O., Meinen, C. S., Collins, J. and Bryden, H. L.: Measuring the
18   Atlantic Meridional Overturning Circulation at 26˚N, Prog. Oceanogr., 130, 91–
19   111, doi:10.1016/j.pocean.2014.10.006, 2015.

20   McPhaden, M. J., Zebiak, S. E. and Glantz, M. H.: ENSO as an integrating concept in
21   earth science, Science, 314(5806), 1740–1745, doi:10.1126/science.1132588,
22   2006.

23   Meehl, G. A., Moss, R., Taylor, K. E., Eyring, V., Stouffer, R. J., Bony, S. and Stevens,
24   B.: Climate model intercomparisons: Preparing for the next phase, Eos, 95(9),
25   77–78, doi:10.1002/2014EO090001, 2014.

26   Mellor, G. L. and Yamada, T.: Development of a turbulence closure model for
27   geophysical fluid problems, Rev. Geophys., 20(4), 851–875,

Geoscientific
Model Development
Discussions

1   doi:10.1029/RG020i004p00851, 1982.

2   Mo, K. C. and Peagle, J. N.: The Pacific-South American modes and their downstream
3   effects, Int. J. Climatol, 21(10), 1211–1229, doi:10.1002/joc.685, 2001.

4   Morice, C. P., Kennedy, J. J., Rayner, N. A. and Jones, P. D.: Quantifying uncertainties
5   in global and regional temperature change using an ensemble of observational
6   estimates: The HadCRUT4 data set, J. Geophys. Res. Atmos., 117(8), 1–22,
7   doi:10.1029/2011JD017187, 2012.

8   Newman, M., Alexander, M. A., Ault, T. R., Cobb, K. M., Deser, C., Di Lorenzo, E.,
9   Mantua, N. J., Miller, A. J., Minobe, S., Nakamura, H., Schneider, N., Vimont,
10   D. J., Phillips, A. S., Scott, J. D. and Smith, C. A.: The Pacific decadal
11   oscillation, revisited, J. Clim., 29(12), 4399–4427, doi:10.1175/JCLI-D-15-
12   0508.1, 2016.

13   Ning, L. and Bradley, R. S.: NAO and PNA influences on winter temperature and
14   precipitation over the eastern United States in CMIP5 GCMs, Clim. Dyn., 46(3–
15   4), 1257–1276, doi:10.1007/s00382-015-2643-9, 2016.

16   Nobre, P., Shukla. J.: Variation of Sea surface Temperature, Wind Stress, and Rainfall
17   over the Tropical Atlantic and South America, J. Clim., 9, 2464–2479,
18   doi:http://dx.doi.org/10.1175/1520-0442(1996)009<2464:VOSSTW>2.0.CO;2,
19   1996.

20   Nobre, P., Marengo, J. A., Cavalcanti, I. F. A., Obregon, G., Barros, V., Camilloni, I.,
21   Campos, N. and Ferreira, A. G.: Seasonal-to-decadal predictability and
22   prediction of South American climate, J. Clim., 19(23), 5988–6004,
23   doi:10.1175/JCLI3946.1, 2006.

24   Nobre, P., De Almeida, R. A., Malagutti, M. and Giarolla, E.: Coupled ocean-
25   atmosphere variations over the South Atlantic Ocean, J. Clim., 25(18), 6349–
26   6358, doi:10.1175/JCLI-D-11-00444.1, 2012.

27   Nobre, P., Siqueira, L. S. P., De Almeida, R. A. F., Malagutti, M., Giarolla, E., Castelã

1   O, G. P., Bottino, M. J., Kubota, P., Figueroa, S. N., Costa, M. C., Baptista, M.,
2   Irber, L. and Marcondes, G. G.: Climate simulation and change in the brazilian
3   climate model, J. Clim., 26(17), 6716–6732, doi:10.1175/JCLI-D-12-00580.1,
4   2013.

5   Nogués-Paegle, J. and Mo, K. C.: Alternating Wet and Dry Conditions over South
6   America during Summer, Mon. Weather Rev., 125, 279–291, doi:10.1175/1520-
7   0493(1997)125<0279:AWADCO>2.0.CO;2, 1997.

8   Obukhov, A. M.: Turbulence in an atmosphere with a non-uniform temperature,
9   Boundary-Layer Meteorol., 2(1), 7–29, doi:10.1007/BF00718085, 1971.

10 de Oliveira Vieira, S., Satyamurty, P. and Andreoli, R. V.: On the South Atlantic
11   Convergence Zone affecting southern Amazonia in austral summer, Atmos. Sci.
12   Lett., 14(1), 1–6, doi:10.1002/asl2.401, 2013.

13 Palmer, T. N., Doblas-Reyes, F. J., Weisheimer, A. and Rodwell, M. J.: Toward
14   seamless prediction: Calibration of climate change projections using seasonal
15   forecasts, Bull. Am. Meteorol. Soc., 89(4), 459–470, doi:10.1175/BAMS-89-4-
16   459, 2008.

17 Richter, I.: Climate model biases in the eastern tropical oceans: Causes, impacts and
18   ways forward, Wiley Interdiscip. Rev. Clim. Chang., 6(3), 345–358,
19   doi:10.1002/wcc.338, 2015.

20 Richter, I., Xie, S. P., Behera, S. K., Doi, T. and Masumoto, Y.: Equatorial Atlantic
21   variability and its relation to mean state biases in CMIP5, Clim. Dyn., 42(1–2),
22   171–188, doi:10.1007/s00382-012-1624-5, 2014.

23 Robertson, A. and Mechoso, C.: Interannual and interdecadal variability of the South
24   Atlantic Convergence Zone, Mon. Weather Rev., 128(8), 2947–2957,
25   doi:10.1175/1520-0493(2000)128<2947:IAIVOT>2.0.CO;2, 2000.

26 Rogers, J. C. and van Loon, H.: Spatial Variability of Sea Level Pressure and 500 mb
27   Height Anomalies over the Southern Hemisphere, Mon. Weather Rev., 110(10),

Geoscientific
Model Development
Discussions

1   1375–1392, doi:10.1175/1520-0493(1982)110<1375:SVOSLP>2.0.CO;2, 1982.

2   Rossow, W. B. and Schiffer, R. a: Advances in Understanding Clouds from ISCCP,
3   Bull.   Amer.   Meteor.   Soc.,   80(11),   2261–2287,   doi:10.1175/1520-
4   0477(1999)080<2261:AIUCFI>2.0.CO;2, 1999.

5   von Storch, H.: Climate models and modeling: an editorial essay, Wiley Interdiscip.
6   Rev. Clim. Chang., 1(3), 305–310, doi:10.1002/wcc.12, 2010.

7   Straus, D. M. and Shukla, J.: Does ENSO force the PNA?, J. Clim., 15(17), 2340–2358,
8   doi:10.1175/1520-0442(2002)015<2340:DEFTP>2.0.CO;2, 2002.

9   Sutton, R. T. and Hodson, D. L. R.: Atlantic Ocean Forcing of North American and
10   European   Summer   Climate,   Science,   309(5731),   115–118,
11   doi:10.1126/science.1109496, 2005.

12   Tarasova, T. A., Barbosa, H. M. J. and Figueroa, S. N.: In- corporation of new solar
13   radiation scheme into CPTECGCM. Instituto Nacional de Pesquisas Espaciais
14   Tech. Rep. INPE- 14052-NTE/371, 44 pp. [Available online at http://mtc-m15.
15   sid.inpe.br/col/sid.inpe.br/iris%401915/2006/01.16.10.40/doc/publicacao.pdf,
16   2006.

17   Tian, B.: Spread of model climate sensitivity linked to double-Intertropical
18   Convergence Zone bias, Geophys. Res. Lett., 42(10), 4133–4141,
19   doi:10.1002/2015GL064119, 2015.

20   Tian, B., Fetzer, E. J., Kahn, B. H., Teixeira, J., Manning, E. and Hearty, T.: Evaluating
21   CMIP5 models using AIRS tropospheric air temperature and specific humidity
22   climatology,   J.   Geophys.   Res.   Atmos.,   118(1),   114–134,
23   doi:10.1029/2012JD018607, 2013.

24   Tiedtke, M.: The sensitivity of the time-mean large-scale flow to cumulus convection in
25   the ECMWF model. Proc. Work-shop on Convection in Large-Scale Models,
26   Reading, United Kingdom, ECMWF, 297–316, 1983.

27   Wallace, J. M. and Gutzler, D. S.: Teleconnections in the Geopotential Height Field

1   during the Northern Hemisphere Winter, Mon. Weather Rev., 109(4), 784–812,

2   doi:10.1175/1520-0493(1981)109<0784:TITGHF>2.0.CO;2, 1981.

3 Wang, C., Zhang, L. and Lee, S.: A global perspective on CMIP5 climate model biases,

4   Nat. Clim. Chang., 4(3), 201–205, doi:10.1038/NCLIMATE2118, 2014.

5 Wanner, H., Brönnimann, S., Casty, C., Luterbacher, J., Schmutz, C. and David, B.:

6   North Atlantic Oscillation – Concepts and Studies, Surv. Geophys., 22(1984),

7   321–382, doi:10.1023/A:1014217317898, 2001.

8 Weaver, A. J., Sedláček, J., Eby, M., Alexander, K., Crespin, E., Fichefet, T.,

9   Philippon-Berthier, G., Joos, F., Kawamiy, M., Matsumoto, K., Steinacher, M.,

10   Tachiiri, K., Tokos, K., Yoshimori, M. and Zickfeld, K.: Stability of the Atlantic

11   meridional overturning circulation: A model intercomparison, Geophys. Res.

12   Lett., 39(20), 1–7, doi:10.1029/2012GL053763, 2012.

13 Winton, M.: A reformulated three-layer sea ice model, J. Atmos. Ocean. Technol.,

14   17(4), 525–531, doi:10.1175/1520-0426(2000)017<0525:ARTLSI>2.0.CO;2,

15   2000.

16 Wu, X. and Mao, J.: Interdecadal variability of early summer monsoon rainfall over

17   South China in association with the Pacific Decadal Oscillation, Int. J. Climatol.,

18   doi:10.1002/joc.4734, 2016.

19 Wu, Z., Li, J., Jiang, Z., He, J. and Zhu, X.: Possible effects of the North Atlantic

20   Oscillation on the strengthening relationship between the East Asian Summer

21   monsoon and ENSO, Int. J. Climatol., 32(5), 794–800, doi:10.1002/joc.2309,

22   2012.

23 Xie, S.-P.: A Dynamic Ocean – Atmosphere Model of the Tropical Atlantic Decadal

24   Variability, J. Clim., 12(1), 64–71, 1999.

25 Xie, S. -Ping and Philander, S. G. H.: A coupled ocean-atmosphere model of relevance

26   to the ITCZ in the eastern Pacific, Tellus A, 46(4), 340–350, doi:10.1034/j.1600-

27   0870.1994.t01-1-00001.x, 1994.

Geoscientific
Model Development
Discussions

1 Xue, Y., Sellers, P., Kinter, J. and Shukla, J.: A Simplified Biosphere Model for Global
2   Climate Studies, J. Clim., 4(3), 345–364, doi:10.1175/1520-
3   0442(1991)004<0345:ASBMFG>2.0.CO;2, 1991.

4 Yu, B. and Zwiers, F. W.: The impact of combined ENSO and PDO on the PNA
5   climate: A 1,000-year climate modeling study, Clim. Dyn., 29(7–8), 837–851,
6   doi:10.1007/s00382-007-0267-4, 2007.

7 Yu, R. and Zhou, T.: Impacts of winter-NAO on March cooling trends over subtropical
8   Eurasia continent in the recent half century, Geophys. Res. Lett., 31(12), 3–6,
9   doi:10.1029/2004GL019814, 2004.

10 Yuan, X. and Yonekura, E.: Decadal variability in the Southern Hemisphere, J.
11   Geophys. Res, 116(D19), 1–12, doi:10.1029/2011JD015673, 2011.

12 Zebiak, S. E.: Air–Sea Interaction in the Equatorial Atlantic Region, J. Clim., 6(8),
13   1567–1586, doi:10.1175/1520-0442(1993)006<1567:AIITEA>2.0.CO;2, 1993.

14 Zhang, L. and Wang, C.: Multidecadal North Atlantic sea surface temperature and
15   Atlantic meridional overturning circulation variability in CMIP5 historical
16   simulations, J. Geophys. Res. Ocean., 118(10), 5772–5791,
17   doi:10.1002/jgrc.20390, 2013.

18 Zhang, L., Ma, H. and Wu, L.: Dynamics and mechanisms of decadal variability of the
19   Pacific-South America mode over the 20th century, Clim. Dyn., 46(11–12),
20   3657–3667, doi:10.1007/s00382-015-2794-8, 2016.

21 Zheng, F., Li, J., Clark, R. T. and Nnamchi, H. C.: Simulation and projection of the
22   Southern Hemisphere annular mode in CMIP5 models, J. Clim., 26(24), 9860–
23   9879, doi:10.1175/JCLI-D-13-00204.1, 2013.

24

Geoscientific
Model Development
Discussions

Open Access

EGU

1 **List of Figures**
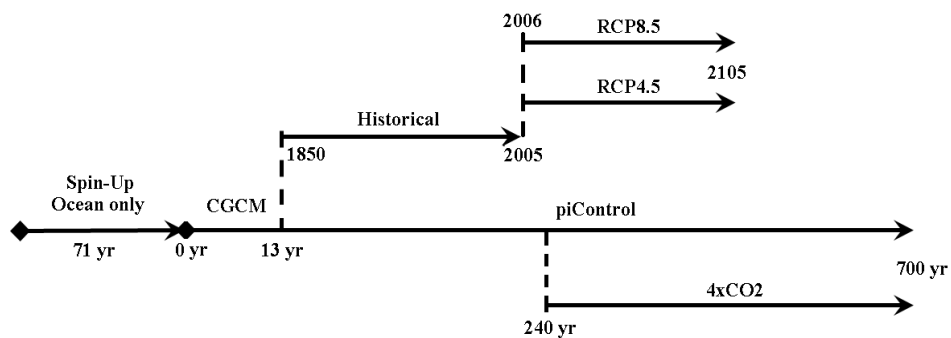
2

3

4 Figure 1 – The scheme of principal simulations carried out by BESM-OA2.5 using

5 different forcing conditions according to CMIP5 protocols. The date for the Historical

6 and RCPs simulations are from actual calendar years.

7 .

8

9

10

Geoscientific
Model Development
Discussions
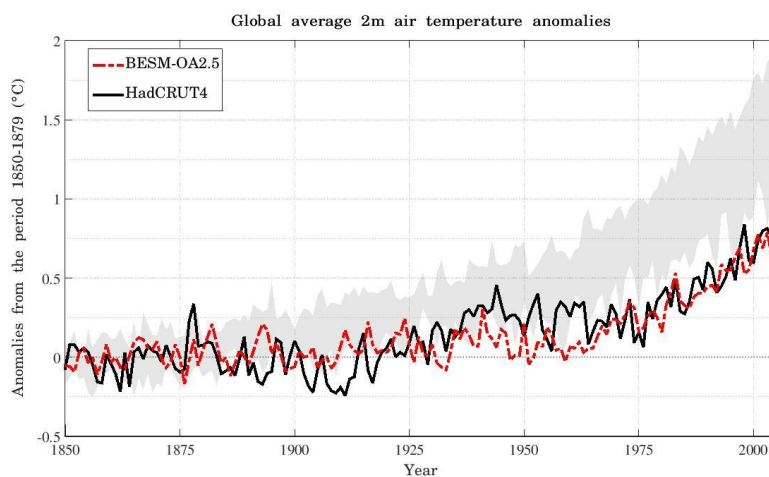
1

2

3   Figure 2 – Global averaged 2-m annual mean air temperature anomalies relative to the

4   period 1850–1879 for BESM-OA2.5 (dashed red line) and observation (solid black

5   line). The grey shadow represents the spread of 11 CMIP5 models (historical GHG

6   simulations). The CMIP5 models anomalies are also computed relative to the period

7   1850–1879, with exception of GFDL-ESM2M and HadGEM2-ES which anomalies are

8   computed relative to the periods 1861−1890 and 1860−1889, respectively. Units are in

9   ℃.

10

11
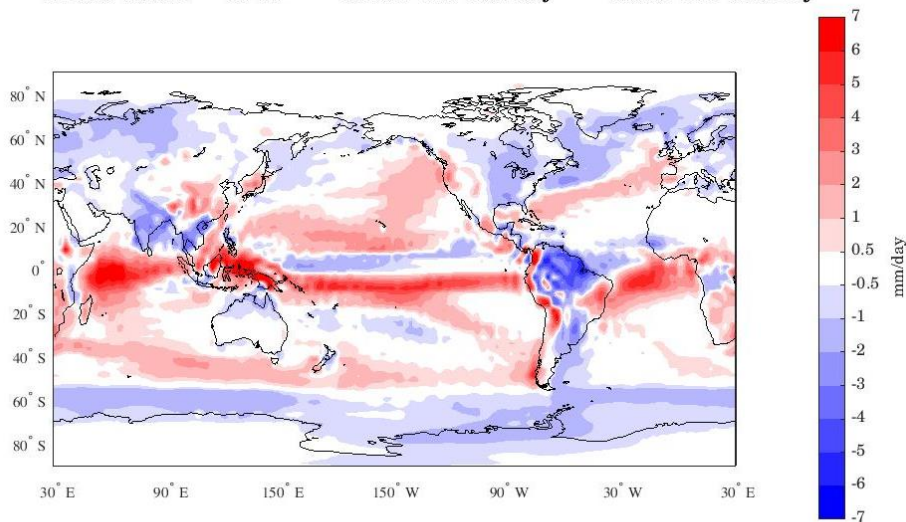
1

2   Figure 3 – Spatial map of annual mean precipitation bias of BESM-OA2.5 relative to

3   GPCP. The averages values are computed over the periods 1971–2000 and 1979–2008,

4   for BESM-OA2.5 and GPCP, respectively. Units are in mm day^{-1}.

5

6

7

8

9

Geoscientific
Model Development
Discussions
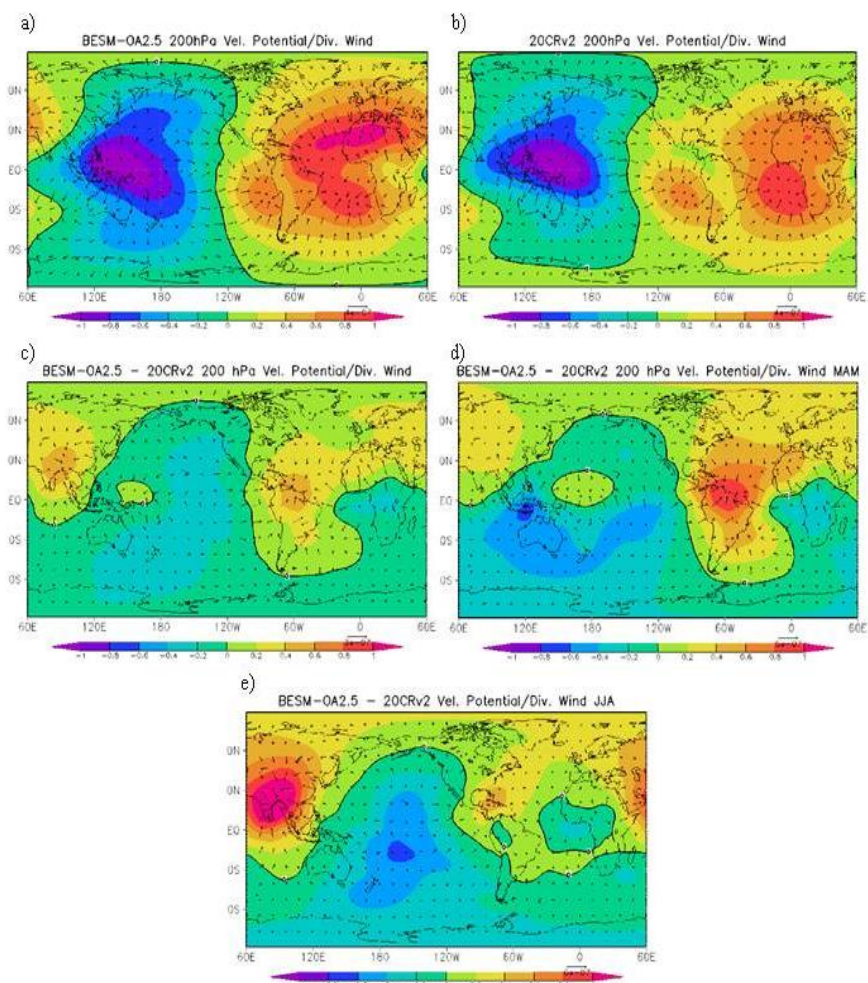
1

2   Figure 4 – Spatial maps with averaged global anomalies of velocity potential and wind

3   divergence at 200 hPa pressure level for (a) BESM-OA2.5 and (b) Reanalysis. (c) The

4   bias of the model relative to the Reanalysis, (d) and (e) are the bias for MAM and JJA

5   seasons, respectively. The averages are computed over the period 1950–2005. Units are

6   in m s^{-1}.

1

2
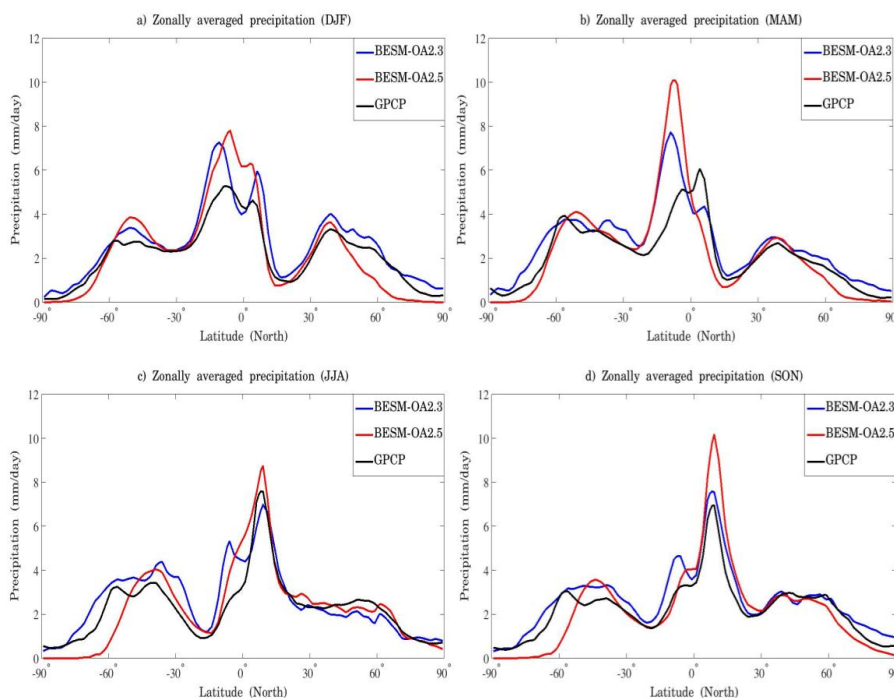
Figure 5 – Zonally averaged annual mean precipitation for BESM-OA2.5, BESM-
OA2.3 and GPCP dataset relative to the seasons DJF, MAM, JJA and SON. The zonally
averages values are computed over the periods 1971–2000 and 1979–2008, for BESM-
OA2.5 and GPCP, respectively. Units are in mm day^{-1}.

7

8

9

10

Geoscientific
Model Development
Discussions

Figure 6 – (a) Spatial map of annual mean total cloud fraction bias of BESM-OA2.5

relative to ISCCP. (b) Zonally averaged total cloud cover for BESM-OA2.5 and ISCCP

dataset. The periods used are 1971–2000 and 1984–2009 for BESM-OA2.5 and ISCCP,

respectively. Units are in percentage.
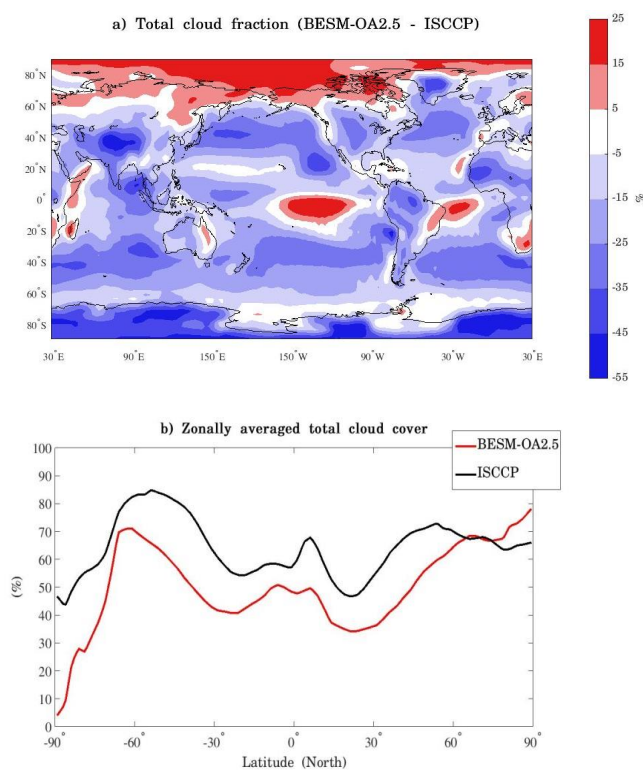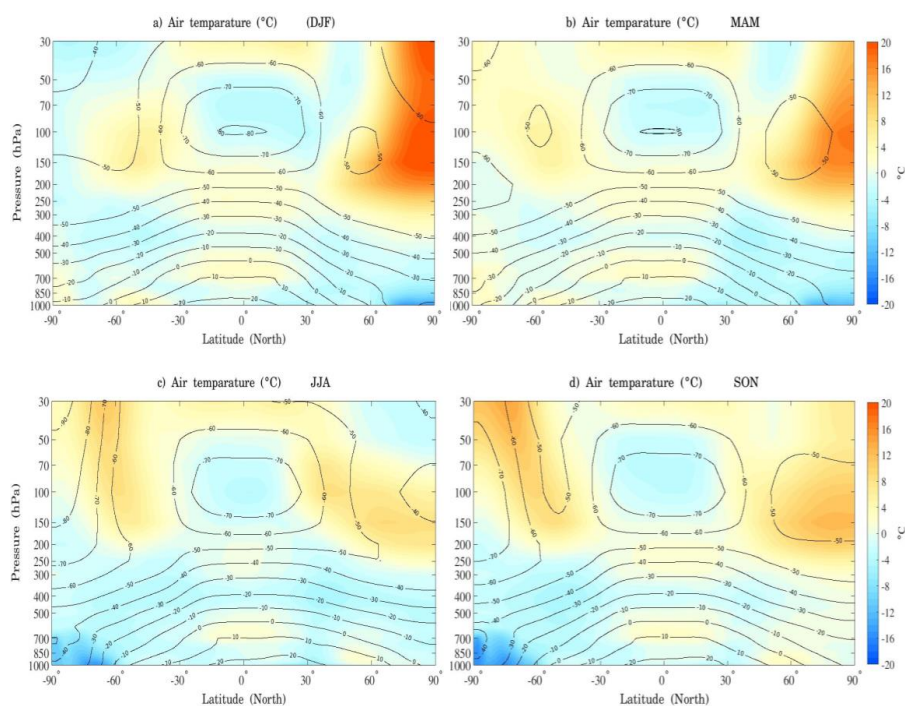
1

2

3   Figure 7 – Contour lines are the zonally averaged vertical air temperature for BESM-

4   OA2.5 and in shaded are the difference BESM-OA2.5 - 20CRv2 data set. Both are

5   averaged over the period 1971–2000. The units are in ℃ and the contour interval is 10

6   ℃.

7

8

9

10

11

Geoscientific
Model Development
Discussions

1

2
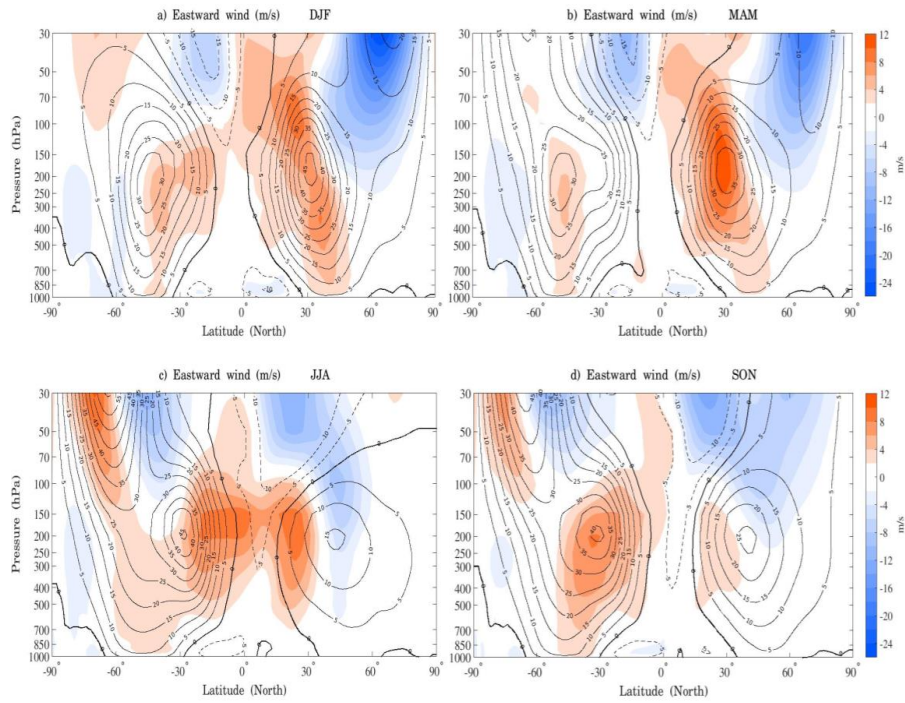
3   Figure 8 – Contour lines are the zonally averaged zonal wind for BESM-OA2.5 and in

4   shaded are the difference BESM-OA2.5 - 20CRv2 data set. Both are averaged over the

5   period 1971–2000. The solid contour lines represent eastward zonal wind and the

6   dashed contour lines represents westward zonal wind. The units are in meters per

7   second and the contour interval is 5 m s^{-1}, with the contour line zero highlighted.

8
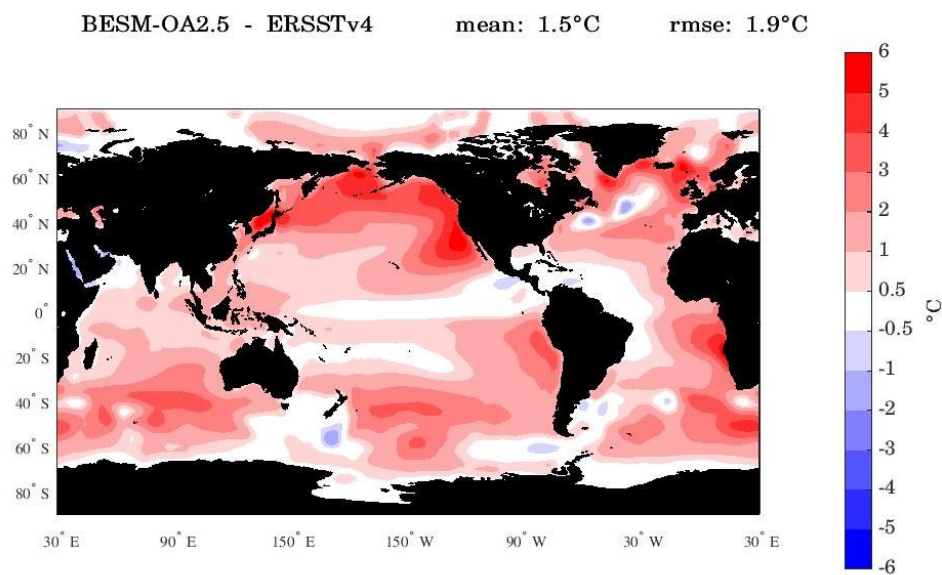
1

2   Figure 9 – Spatial map of annual mean sea surface temperature bias of BESM-OA2.5

3   relative to ERSSTv4. The averages are computed over the period 1971–2000. Units are

4   in ℃.

5

6

7

8

9

a) Equatorial Pacific Mean SST

b) BESM-OA2.5
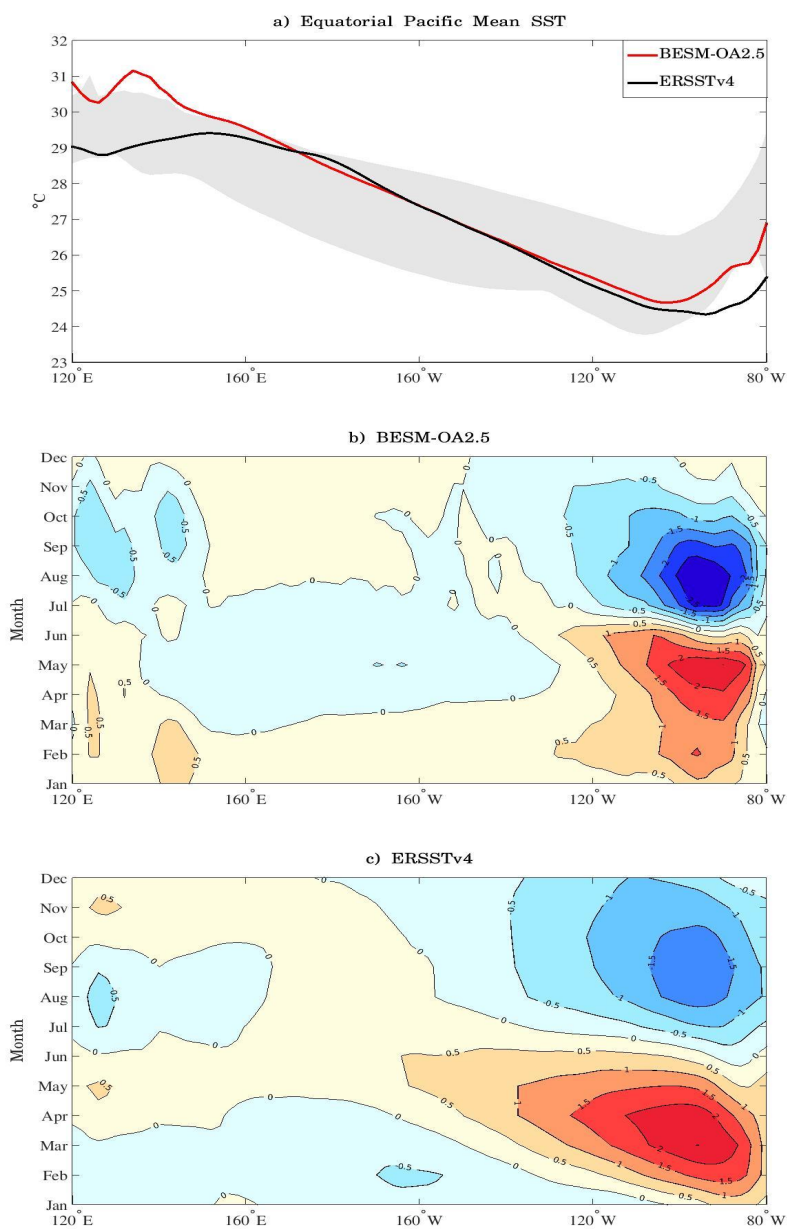
c) ERSSTv4

1

2

3

1   Figure 10 – (a) Mean SST along the equator in the Pacific Ocean and annual cycle of

2   the equatorial Pacific SST anomalies for (b) BESM-OA2.5 and (c) ERSSTv4.

3   Equatorial region is defined by averaging over 2 ºS–2 ºN. BESM-OA2.5 and ERSSTv4

4   are averaged over the period 1971–2000. In (a) the grey shadow represents the spread of

5   11 CMIP5 models, which are also averaged over the period 1971–2000. Units are in ℃.
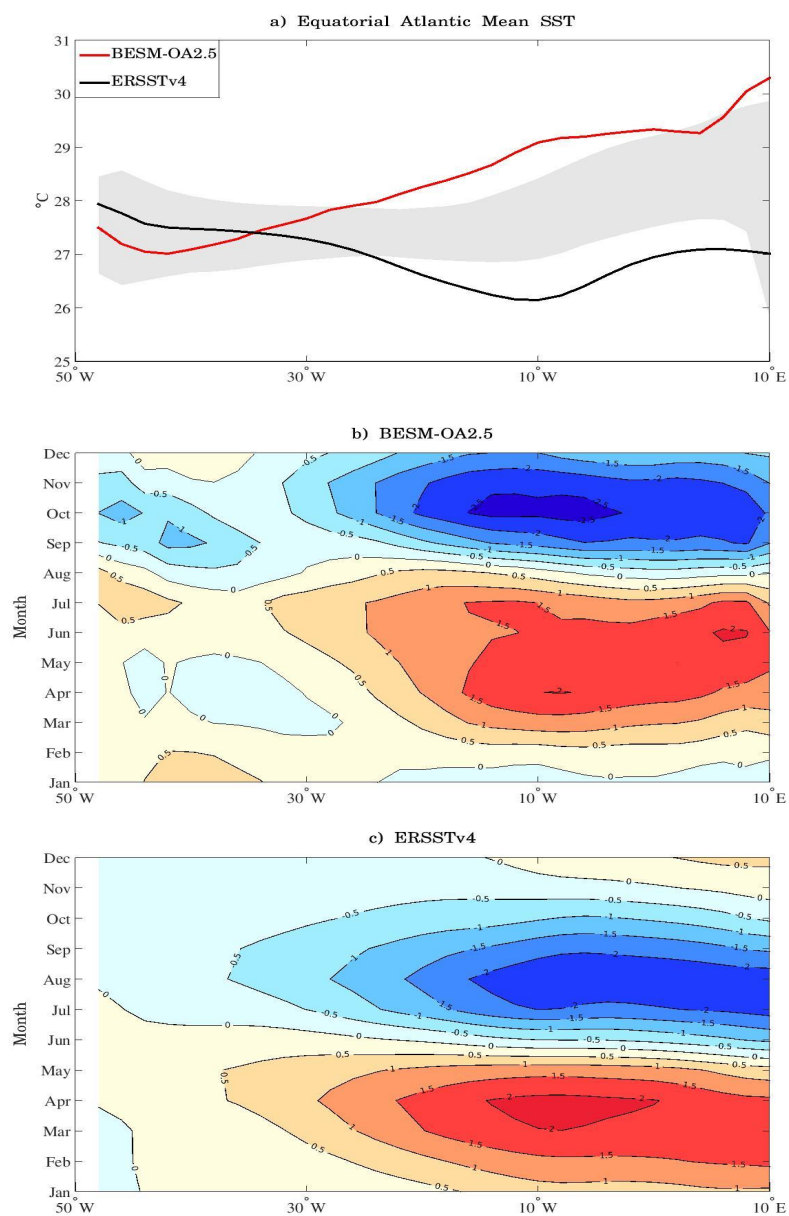
1

2

3   Figure 11 – As Fig. 10 but for the Atlantic Ocean.

1

2

3

4

5

6

7

8
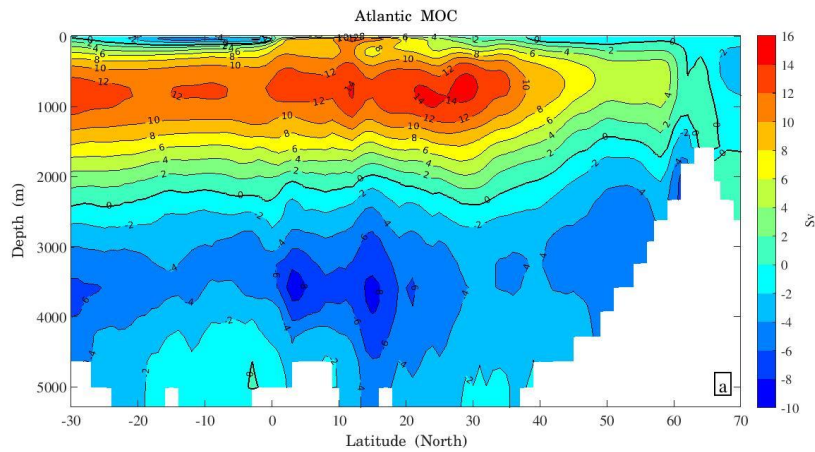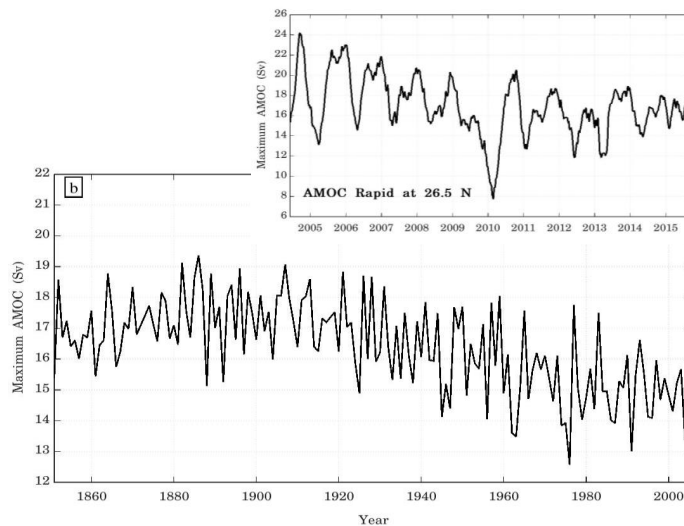
Figure 12 – (a) Atlantic Meridional Overturning Circulation averaged for the period

1971–2000 and (b) annual mean maximum AMOC strength time series at the latitude

30 °N simulated by BESM-OA2.5 for historical simulation over the period 1850–2005.

The smaller graph shows the AMOC time series measured by the project RAPID at

26.5 ° N over the period April/2004 to October/2015. The RAPID time series is

smoothed by a 3-month running average. Units are in Sverdrup.

1

2
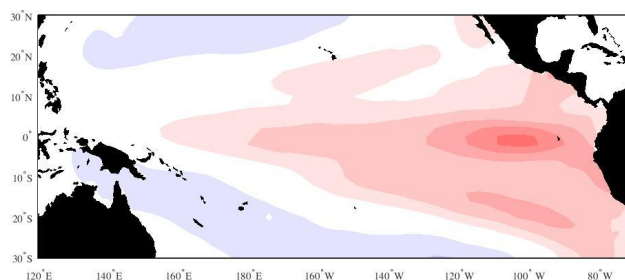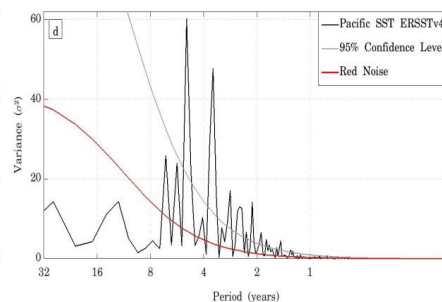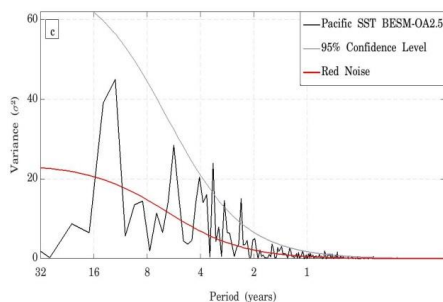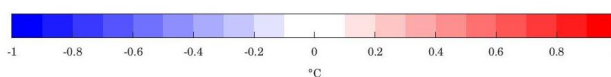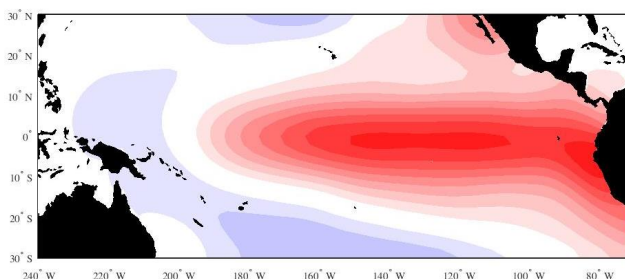
Figure 13 – The leading EOF modes of the detrended monthly SST anomalies over the

Tropical Pacific region (30 ° S–30 ° N; 240 °–70 ° W) for (a) BESM-OA2.5 and (b)

ERSSTv4. The results are shown as the SST anomalies regressed onto the

1   corresponding normalized PC time series (℃ per standard deviation) over the period

2   1950–2005. The percentage of the variance explained by each EOF is indicated in the

3   title of the figure. The contour interval is 0.1 ℃. Figures (c) and (d) are the power

4   spectrum of the leading joint PC time series of the pattern for BESM-OA2.5 and

5   ERSSTv4, respectively. The solid red line represents the theoretical red noise spectrum

6   and the gray line represents the 95 % confidence level.

7

8

9

10

11

12
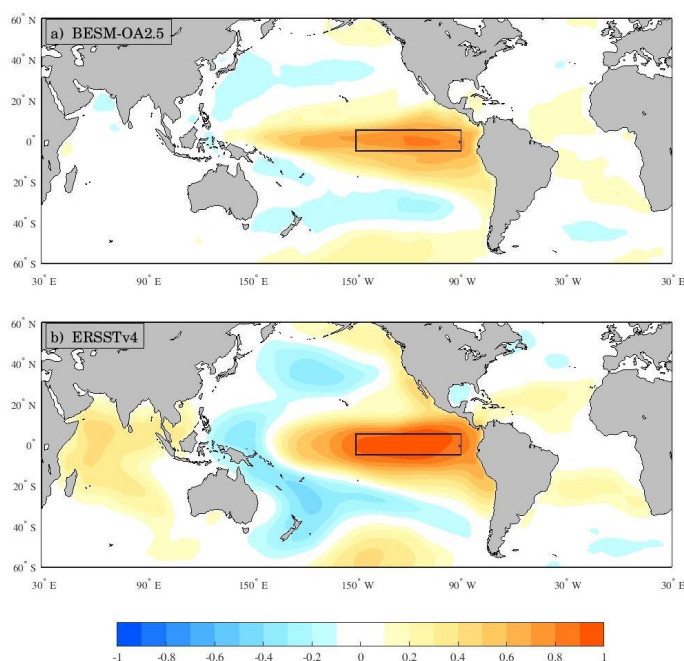
Figure 14 – Spatial maps with the monthly correlation between Niño-3 index and global SST anomalies computed for (a) BESM-OA2.5 and (b) ERSSTv4 over the period 1900–2005. The anomalies are obtained by subtracting the monthly means for the whole detrended time series at each grid point. Black rectangles show the Niño-3 index region. Shaded areas are statistically significant at the 95 % confidence level (through two tailed t-student test).
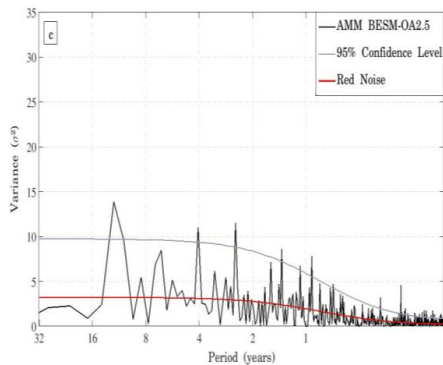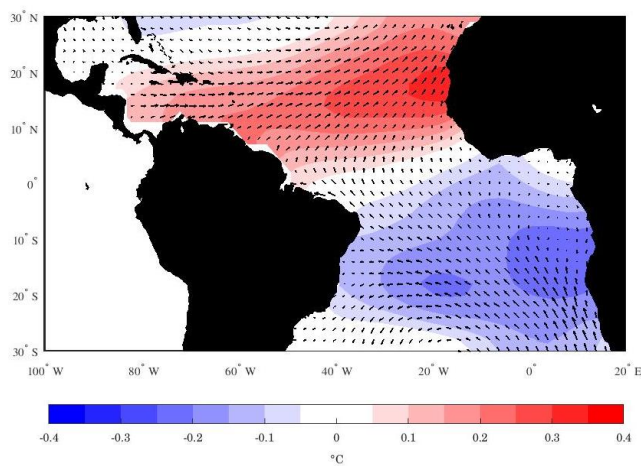
Geoscientific
Model Development
Discussions

a) AMM jEOF1 (10.7%) BESM-OA2.5
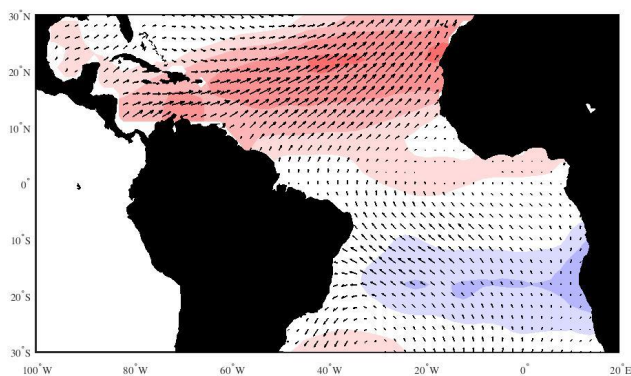
b) AMM jEOF1 (11.8%) ERSSTv4 (SST), 20CRv2 (Taux,Tauy)

1

Geoscientific
Model Development
Discussions
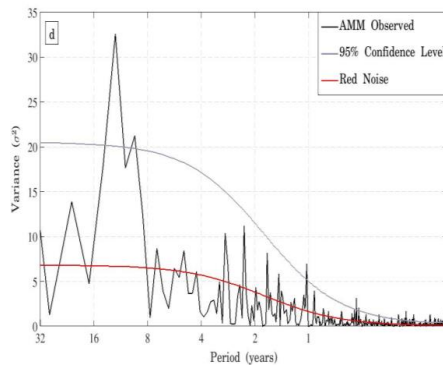
1   Figure 15 – The leading joint EOF modes of the detrended monthly SST and wind stress

2   (Taux and Tauy) anomalies for the Tropical Atlantic region (30 °S–30 °N; 100 °W–20 °

3   E) for (a) BESM-OA2.5 and (b) for observation (ERSSTv4 and 20CRv2 Reanalysis).

4   The results are shown as the SST anomalies regressed onto the corresponding

5   normalized PC time series (°C per standard deviation) and wind stress anomalies

6   regressed onto the corresponding normalized PC time series (ms^{-1} per standard

7   deviation) over the period 1950–2005. The percentage of the variance explained by each

8   EOF is indicated in the title of the figure. The contour interval is 0.05 °C. Figures (c)

9   and (d) are the power spectrum of the leading joint PC time series of the AMM pattern

10 for BESM-OA2.5 and observation, respectively. The solid red line represents the

11 theoretical red noise spectrum and the gray line represents the 95 % confidence level.
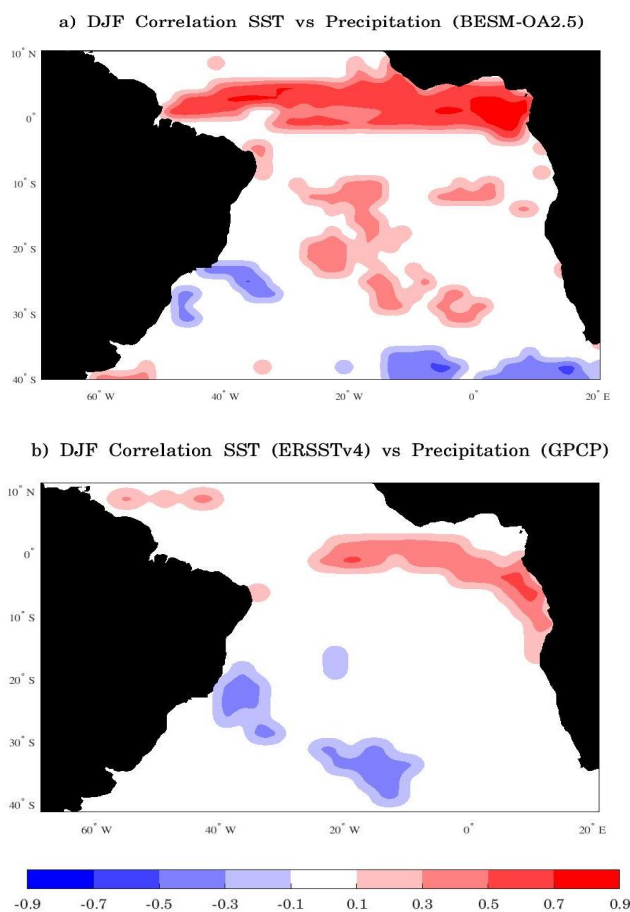
12

13

14

15

16

17

18

19

20

21

1

a) DJF Correlation SST vs Precipitation (BESM-OA2.5)

b) DJF Correlation SST (ERSSTv4) vs Precipitation (GPCP)

Figure 16 – Spatial maps with the correlation between SST and precipitation (seasonal average DJF) over the South Ocean (40º S−10º N; 70º W−20º E) computed for (a) BESM-OA2.5 over the period 1971−2002 and (b) observations over the period 1979−2010. Shaded areas are statistically significant at the 95 % confidence level (through two tailed t-student test).
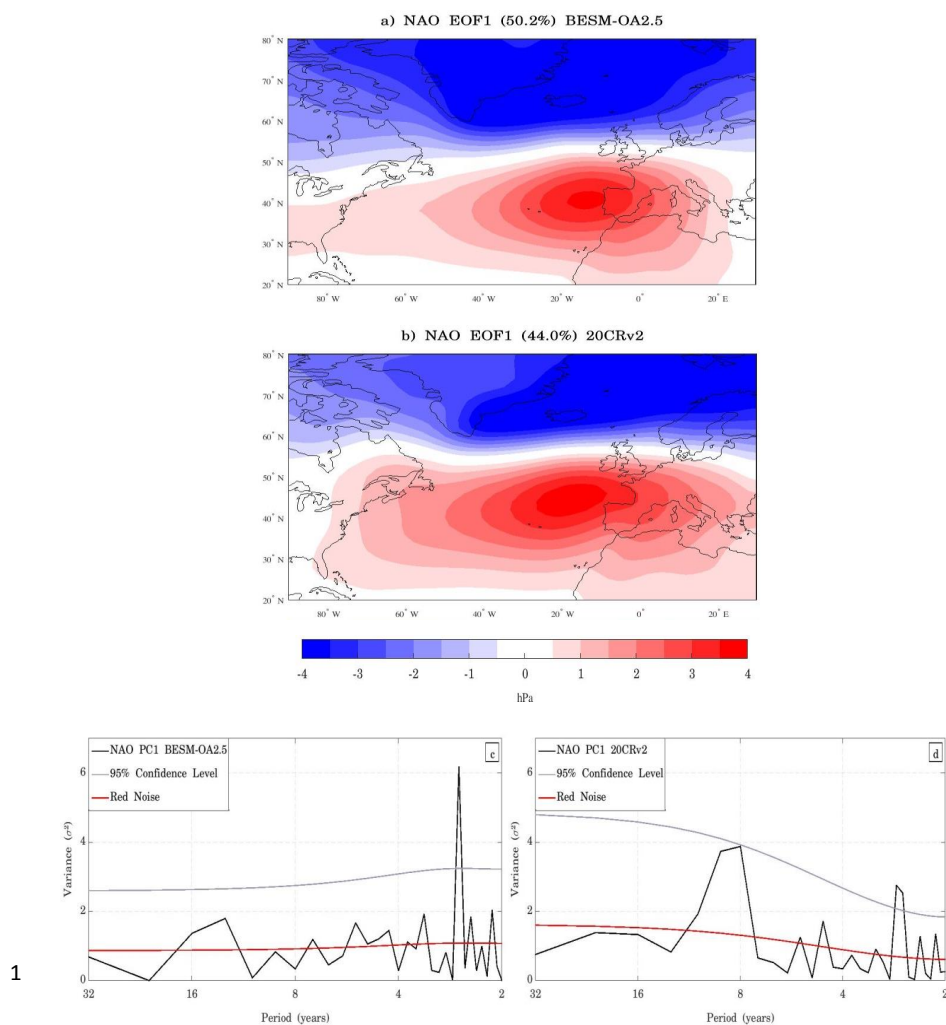
1

2

3   Figure 17 – The leading EOF modes of the boreal winter (DJF) seasonal averaged SLP

4   anomalies for the Euro-Atlantic region (20º−80º N; 100º W−30º E) for (a) BESM-

5   OA2.5 and (b) 20CRv2. The results are shown as the SLP anomalies regressed onto the

6   corresponding normalized PC time series (hPa per standard deviation) for the period

7   1950−2005. The percentage of the variance explained by each EOF is indicated at the

Geoscientific
Model Development
Discussions

1   title of the figure. The contour interval is 0.5 hPa. Figures (c) and (d) are the power

2   spectrum of the leading PC time series of the NAO pattern for BESM-OA2.5 and

3   20CRv2, respectively. The solid red line represents the theoretical red noise spectrum

4   and the gray line represents the 95 % confidence level.

5

6

7

8

9

10

11

12

13

14

15

16

17

18

19

20

21

22

23

24

25

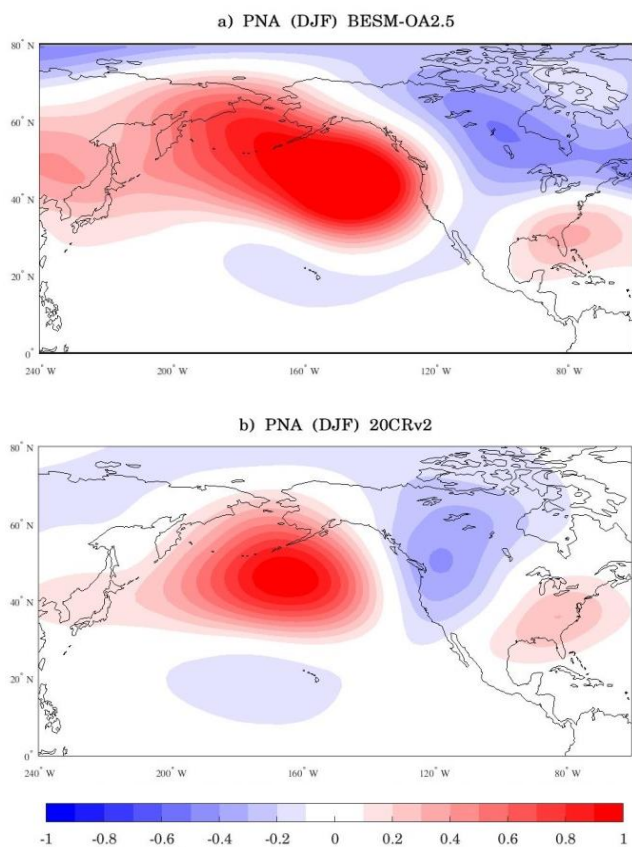Figure 18 – One-point correlation map for (a) BESM-OA2.5 and (b) 20CRv2 Reanalysis showing the correlation coefficient of 500 hPa geopotential level based at 45 ºN, 165 ºW and the other grid points. The time series used are boreal winter seasonal (DJF) averaged dataset for the period 1950−2005.

Geoscientific
Model Development
Discussions

1

Figure 19 – (a) The second and third EOF modes of the monthly mean 500 hPa geopotential height field for the Southern Hemisphere (20º−90º S) for BESM-OA2.5 (b) and for 20CRv2 Reanalysis. The results are shown as the 500 hPa geopotential height regressed onto the corresponding normalized PC time series (meters per standard deviation) over the period 1950−2005. The percentage of the variance explained by each EOF is indicated at the title of the figure. The contour interval is 10 m.
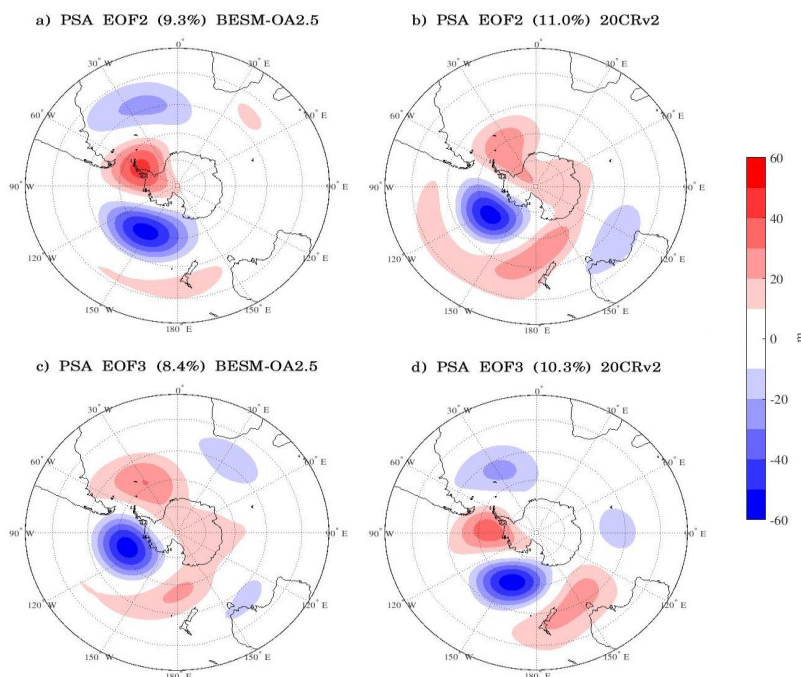
1

2

3

4

5

6

7

8

9

10

Figure 20 – The leading EOF modes of the monthly mean 500 hPa geopotential height field for the Southern Hemisphere (20º−90º S) for (a) BESM-OA2.5 and (b) for 20CRv2 Reanalysis. The results are shown as the 500 hPa geopotential height regressed onto the corresponding normalized PC time series (meters per standard deviation) over the period 1950−2005. The percentage of the variance explained by each EOF is indicated at the title of the figure. The contour interval is 10 m.
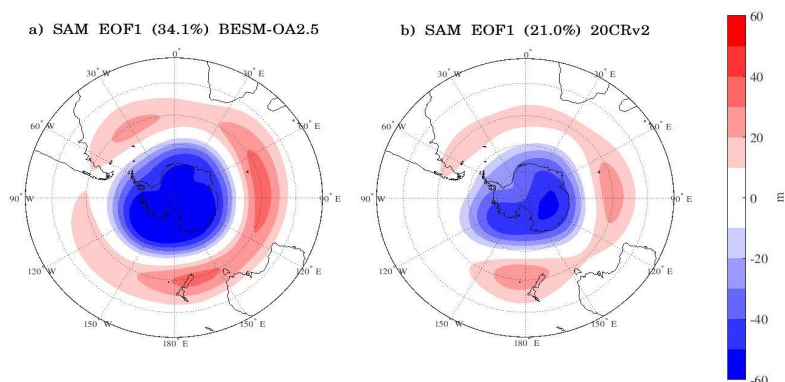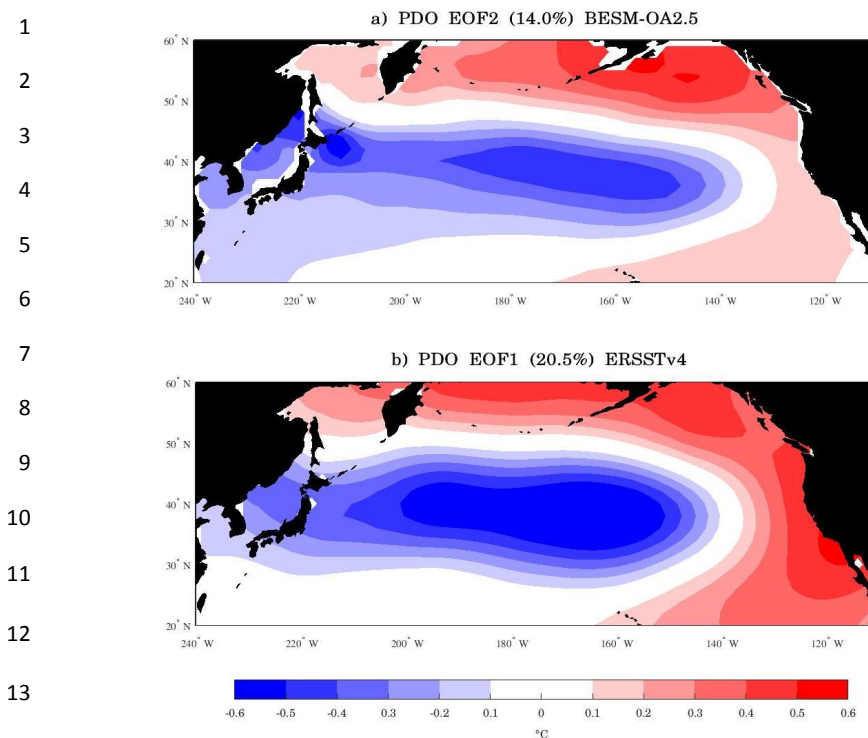
17

18

19

20

21

22

23

24

25

Figure 21 − (a) The second EOF mode of monthly SST anomalies of BESM-OA2.5 and (b) the leading EOF mode of monthly SST anomalies of ERSSTv4, both over North Pacific Ocean (20º−60º N; 240º−110º W). The results are shown as the monthly SST anomalies regressed onto the corresponding normalized PC time series (℃ per standard deviation) over the period 1900−2005. The percentage of the variance explained by each EOF is indicated at the title of the figure. The contour interval is 0.1 ℃.
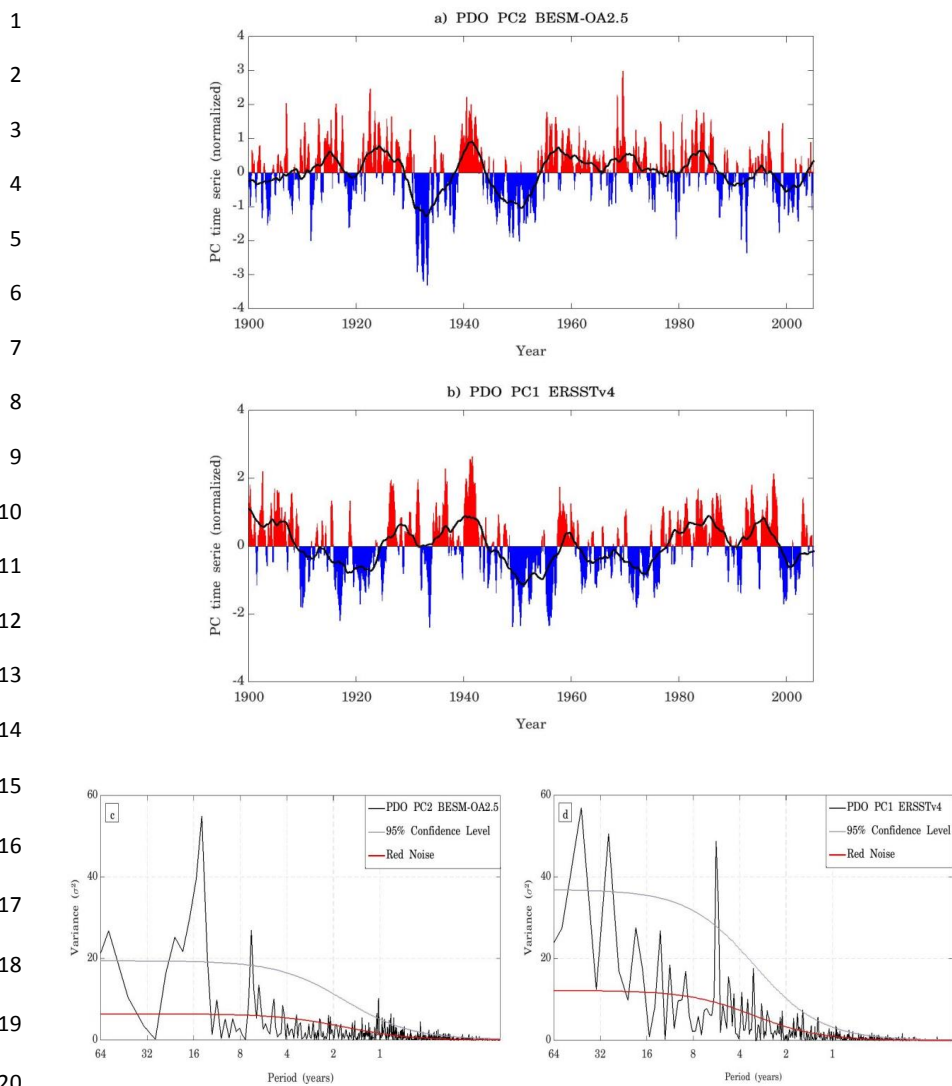
Figure 22 – Normalized second PC time series for (a) BESM-OA2.5 and normalized

leading PC time series for (b) ERSSTv4 over the period 1900–2005. The solid black

lines are the 5-year running average. Figures (c) and (d) are the power spectrum of the

second PC time series for BESM-OA2.5 and for the leading PC time series for 20CRv2,

1   respectively. The solid red line represents the theoretical red noise spectrum and the

2   gray line represents the 95 % confidence level.

3

4

5

6

7

8

9

10

11

12

13

14

15

16

17

18

19

20

21

22

23

24

25

Geoscientific
Model Development
Discussions

Institute	Model	Simulation	horizontal resolution (lat ×lon)	
			Atmosphere	Ocean
Commonwealth Scientific and Industrial Research Organisation/Bureau of Meteorology (Australia)	ACCESS1.3	Historical GHG r3i1p1	1.25 °×1.875 °	300 ×360 (tripolar)
Canadian Centre for Climate Modelling and Analysis (Canada)	CanESM2	Historical GHG r1i1p1	2.7906 °×2.8125 °	0.9303 °; 1.1407 °×1.40625 °
National Center for Atmospheric Research (USA)	CCSM4	Historical GHG r1i1p1	0.9424 °×1.25 °	384 ×320 (tripolar)
Centre National de Recherches Météorologiques/Centre Européen de Recherche et de Formation Avancée en Calcul Scientifique (France)	CNRM-CM5	Historical GHG r1i1p1	1.4008 °×1.40625 °	292 ×362 (tripolar)
Geophysical Fluid Dynamics Laboratory (USA)	GFDL-ESM2M	Historical GHG r3i1p1	2.0225 °×2.5 °	0.3344 °; 1 °×1 °
Goddard Institute for Space Studies (USA)	GISS-E2-H	Historical GHG r1i1p1	2 °×2.5 °	1 °×1 °
Met Office Hadley Centre (UK)	HadGEM2-ES	Historical GHG r1i1p1	1.25 °×1.875 °	0.3396 °; 1 °×1 °
L'Institut Pierre-Simon Laplace (France)	IPSL-CM5A-MR	Historical GHG r1i1p2	1.2676 °×2.5 °	149 ×182 (tripolar)
Japan Agency for Marine-Earth Science and Technology, Atmosphere and Ocean Research Institute (The University of Tokyo), and National Institute for Environmental Studies (Japan)	MIROC-ESM	Historical GHG r1i1p1	2.7906 °×2.8125 °	0.5582 °; 1.7111 °×1.40625 °
Meteorological Research Institute (Japan)	MRI-CGCM3	Historical GHG r1i1p1	1.12148 °×1.125 °	0.5 °; 0.5 °×1 °
Bjerknes Centre for Climate Research and Norwegian Meteorological Institute (Norway)	NorESM1-M	Historical GHG r1i1p1	1.8947 °×2.5 °	384 ×320 (tripolar)

1

2   Table 1 - List of models from CMIP5 with historical GHG simulations used to compare

3   with BESM-OA2.5. Models with higher resolution in the tropical region and a

1   decreasing resolution towards the poles have two values for latitude in their respective

2   oceanic resolution column. Models with oceanic tripolar grid, the number of grid points

3   in each coordinate are presented.

4

5